CHAPTER XII

NEW PARTICLES AND THEIR EXPERIMENTAL SIGNATURES

J. Ellis, G. Gelmini and H. Kowalski

NEW PARTICLES AND THEIR EXPERIMENTAL SIGNATURES

J. Ellis and G. Gelmini
CERN, Geneva, Switzerland

H. Kowalski
DESY, Hamburg, Fed. Rep. Germany

1. Introduction

The most exciting experiments with a new accelerator are those which discover new particles. One of the main motivations for a Large Hadron Collider in the LEP tunnel is the opportunity it offers for exploring a new energy range, and perhaps discovering new particles with masses up to O(1) TeV. This report summarizes work done by our theoretical working group on exotic particles before, during and since the Lausanne meeting. We discuss the motivations, rates and experimental signatures for new physics and new particles in the 1 TeV mass range.

Section 2 reviews some of the motivations for expecting new physics in this range. Of particular interest is the physics of gauge symmetry breaking. From where do the $W^{\pm}$ and Z° acquire their masses? From spontaneous symmetry breaking? Via the Higgs mechanism with elementary Higgs particles? Are Higgs masses protected by supersymmetry? Or are they composite? Other ideas for new physics which might be detectable in the 1 TeV range include the possibility that the $W^{\pm}$ and Z° may be composite - is this why they are massive, whilst the photon γ and gluon g are massless? - or that quarks and leptons may be composite - is this why there are so many flavours of apparently "fundamental" fermions? In the case of spontaneous gauge symmetry breaking it is possible to give firm arguments why new physics should be expected in the 1 TeV range. Such may also be the case in models with composite $W^{\pm}$ and Z°. It is not so obvious why quarks and leptons should appear composite at an energy scale O(1) TeV, although some theorists have been inspired by recent UAn collider data [2,3,4,5,6] to speculate about this possibility. More motivations for new physics in the 1 TeV range are provided by Riccardo Barbieri [7] in his talk at this meeting, while Roberto Peccei [8] discusses composite models in his talk. One possibility (discussed at this meeting by Chris Llewellyn Smith[9]) is an extension beyond $SU(2)_L \times U(1)_Y$ of the electroweak gauge group, perhaps to $SU(2)_L \times SU(2)_R \times U(1)$, which some theorists expect to yield new gauge bosons with masses below 1 TeV.

In section 3 we discuss the rates and experimental signatures of new particles predicted by theoretical models of gauge symmetry breaking, notably the Higgs boson, supersymmetry and technicolour. Among the signatures we discuss are multiple $W^{\pm}$ and/or Z° events (for the Higgs), missing transverse energy (for supersymmetry) and multiple $\bar{t}t$ events

(for the Higgs and technicolour). We provide many examples of final state differential distributions in rapidity and p_T, particularly for Higgses and for supersymmetry. We also analyse some physics backgrounds to the new particle production processes which interest us. Examples include W^+W^-, $Z^\circ Z^\circ$, $W(\bar{t}t)$ and $(\bar{t}t)(\bar{t}t)$ production as backgrounds to Higgs production. However, we do not consider in detail non-physics backgrounds such as the jet fluctuation background to missing energy signals for supersymmetry production. Many calculations of conventional physics processes which may provide backgrounds to new particle production are presented in the talks by Ali [10] and by Andersson [11]. The production of new particles in ep collisions is discussed in the talk by Altarelli [12].

Section 4 summarizes our preliminary conclusions on the observability at a high energy hadron collider of the new particles studied in this report [13].

2. New Physics in the 1 TeV Range?

Unfortunately for our sense of progress, the Standard SU(3) x SU(2) x U(1) Model continues to work very well. Fortunately, the veneer of experimental success may be beginning to crack. In recent months a variety of funny events have been reported from the CERN $p\bar{p}$ Collider. Among these are monojet "zen" events [4,6], electron + jet + missing energy-momentum events [3], anomalous $Z^\circ \to l^+l^-\gamma$ decays [2], a possible bump in the multijet invariant mass distribution around 150 GeV in mass [5], and a number of dimuon events, particularly three with like signs. Many physicists believe that some of these events may be inexplicable within the Standard Model. Perhaps all these phenomena will eventually turn out to be explicable within the Standard Model, but we hope one or more of them may lead us beyond it. Theorists have been proclaiming for some time the inadequacies of the Standard Model, and proposing myriad solutions to the mysteries it leaves unsolved.

What are the origins of particle masses? Are they due to the spontaneous breakdown of $SU(2)_L \times U(1)_Y$? Why is there such a proliferation of "fundamental" quark and lepton flavours? Are they composite? Are the $W^\pm$ and Z° composite? Are the spin-zero fields related to gauge symmetry breaking composite? Since they offer the best motivations for the existence of new physics in the 1 TeV range, we will concentrate here on the possible mechanism of weak gauge symmetry breaking, including the possibility of composite spin-zero fields.

2.1 Gauge Symmetry Breaking

If weak gauge invariance were exact, the $W^\pm$ and Z° would be massless, in the same way that the masslessness of the photon and gluon reflect exact $U(1)_{em}$ and $SU(3)_C$ gauge invariance respectively. Similarly, the known quarks and leptons would have to be massless, since their left- and right-handed components f_L, f_R are known from standard weak interaction phenomenology to have different isospins: $I = \frac{1}{2}$, 0 respectively leading to maximal parity violation in the charged current weak interactions. Fermion mass terms couple left to right: $m_f(\bar{f}_L f_R + \bar{f}_R f_L)$: and therefore must violate weak isospin invariance with $\Delta I = \frac{1}{2}$. Hints on the nature of the new physics responsible for weak gauge symmetry breaking can be extracted from an analysis of perturbative unitarity and renormalizability [14].

To avoid unrenormalizable divergences in one-loop contributions (fig.1) to $2 \leftrightarrow 2$ scattering processes, all tree level $2 \leftrightarrow 2$ scattering cross-sections must fall as $1/E_{cm}^2$ at high energies. The archetype is $e^+e^- \to \mu^+\mu^-$, which is well-known to have the point-like cross-section $4\pi\alpha^2/3E_{cm}^2$ in lowest order QED, consistent with the renormalizability of the theory. Non-abelian gauge theories almost succeed in having the same good behaviour, thanks to the cancellations due to the 3- and 4-gauge boson vertices (fig.2). However, there are residual excesses over the $1/E_{cm}^2$ law, which are proportional to m_f in the case of $f\bar{f} \to W^+W^-$ annihilation, and proportional to m_W^2 in $W^+W^- \to W^+W^-$ scattering. To cancel these out we must introduce (fig.3) a new boson with couplings to fermions $\propto m_f$, and to gauge bosons $\propto m_W^2$. Such a boson should not have spin greater than 1, as the couplings of such particles are well-known to be unrenormalizable. The hypothetical new boson cannot have spin 1, since the only such bosons allowed are gauge bosons, and they have universal couplings to fermions, not couplings proportional to m_f. The only solution [14] is to postulate a new boson with spin zero - either the Higgs boson or something very much like it.

2.2 Elementary Higgses

We have already seen that generic Higgs couplings are proportional to m_f for fermions and to m_W^2 for massive gauge bosons. In the minimal version of the Standard Model with one complex $I = \frac{1}{2}$ Higgs doublet there is just one elementary neutral Higgs H° and no charged Higgs $H^\pm$, and we will stick to this minimal possibility in what follows. The couplings of the unique H° are completely fixed [15]:

$$g_{H\bar{f}f} = (\sqrt{2}\,G_F)^{\frac{1}{2}}\, m_f \ , \quad g_{HW^+W^-} = 2(\sqrt{2}\,G_F)^{\frac{1}{2}}\, m_W^2 \tag{2.1}$$

Thus the H° couples to the heaviest particles available. For example, decay rates to some fundamental quarks and leptons are in the ratios

$$\begin{aligned} &\Gamma(H^\circ \to \bar{t}t) : \Gamma(H^\circ \to \bar{b}b) : \Gamma(H^\circ \to \tau^+\tau^-) : \Gamma(H^\circ \to \mu^+\mu^-) \\ &\approx 3m_t^2 : 3m_b^2 : m_\tau^2 : m_\mu^2 \end{aligned} \tag{2.2}$$

Thus any H° heavy enough to decay into $(\bar{t}t)$ would have a $\mu^+\mu^-$ branching ratio less than 10^{-5}. Thus looking for $H^\circ \to \mu^+\mu^-$ at a large hadron-hadron collider is unlikely to be very fruitful.

While the couplings (2.1) of the minimal H° are completely determined, its mass is almost completely arbitrary. Fruitless nuclear physics searches [16] tell us that

$$m_{H^\circ} \gtrsim O(15)\ \text{MeV} \tag{2.3}$$

while radiative corrections and conventional cosmology [17] suggest that

$$m_{H^\circ} \gtrsim 10\ \text{GeV} \tag{2.4}$$

However, the radiative correction limit is not watertight, and can be evaded if the t quark mass is suitably chosen. At the upper end, if we want the Higgs self-coupling to be weak enough for perturbation theory to be applicable, then we need [18,19]

$$m_{H^\circ} \lesssim O(1)\ \text{TeV} \tag{2.5}$$

Of course, it is just this assumption of weak self-coupling which is jettisoned in technicolour models [20] of strongly interacting composite Higgses. The range (2.3, 2.4, 2.5) is rather wide. We take the point of view that if $m_{H^\circ} < 100$ GeV, it will have been detected[21] at LEP before our large hadron-hadron collider comes into operation. Let us assume also that $m_t \lesssim 50$ GeV. If $2m_t < m_{H^\circ} < 2m_{W^\pm}$ we expect the dominant decay mode of the H° to be into $\bar{t}t$, whereas if $m_{H^\circ} > 2m_{W^\pm}$ or $2m_{Z^\circ}$ we expect the decays into W^+W^- and $Z^\circ Z^\circ$ to dominate (their ratio is 2:1 for $m_{H^\circ} \gg 2m_{Z^\circ}$). Heavy Higgses have a large total decay rate [19]:

$$\Gamma(H^\circ) = \left[\frac{G_F m_W^2}{8\pi\sqrt{2}} \frac{(1 - x_\pm)^{\frac{1}{2}}}{x_\pm} (3x_\pm^2 - 4x_\pm + 4) + \frac{G_F m_W^2}{16\pi\sqrt{2}} \frac{(1 - x_\circ)^{\frac{1}{2}}}{x_\circ} (3x_\circ^2 - 4x_\circ + 4) \right] \tag{2.6}$$

where $x_{\pm,\circ} = 4m^2_{W^\pm, Z^\circ}/m^2_{H^\circ}$, which means that $\Gamma(H^\circ) \to m_{H^\circ}$ as $m_{H^\circ} \to 1$ TeV. The decay rates of heavy Higgses are plotted in fig.4: we see how the $\bar{t}t$ decay mode is overwhelmed when $m_{H^\circ} > 2m_{W^\pm}$. Also shown on fig.4 are lines corresponding to $\Gamma(H^\circ)/m_{H^\circ} = 0.01$ and 0.1. We see that if $m_{H^\circ} < 200$ GeV it is worthwhile aiming for a 1% resolution in m_{H°, since the natural width is smaller. However, if $m_{H^\circ} > 400$ GeV it is not even worthwhile trying to get a mass resolution of 10%, since the natural width of the H° is larger. This means that a massive H° will be more difficult to disentangle from background sources of W^+W^- or $Z^\circ Z^\circ$ production, for example from continuum $q\bar{q} \to W^+W^-$ or $Z^\circ Z^\circ$ production.

Another important source of background will be 2 simultaneous hard parton-parton collisions, either with both giving vector bosons, or with one giving a $W^\pm$ or Z° and the other giving a dijet pair with $m_{jj} \approx 80$ or 90 GeV [22]. As we will see in section 3, typical cross-sections for H° production are O(1)pb, and therefore the rates will not be so generous that we can afford the luxury of working only with leptonic decays of the $W^\pm$ and Z°. Moreover, we lose all kinematic constraints when we look at $(W^+ \to l^+\nu)(W^- \to l^-\nu)$. Therefore we will presumably have to try to work with at least one hadronic $W^\pm$ or Z° decay, and contend with QCD multijet backgrounds. As we will see in more detail in section 3, looking for heavy neutral Higgses in hadron-hadron collisions will not be very easy. Although we do not discuss them here, looking for the charged Higgses present in non-minimal models is probably comparably difficult.

2.3 The Trouble with Higgs

When one calculates loop corrections (fig.5a) to the mass of an elementary Higgs boson, one finds that they are quadratically divergent:

$$\delta m_H^2 \propto \int^{\Lambda} d^4k \frac{1}{k^2} \propto \Lambda^2 \tag{2.7}$$

Some might argue that these divergences are unimportant, because they are renormalizable and can be compensated by a suitable choice of the bare Higgs mass. However, these divergences, if not diseases in themselves, seem to be symptoms of a more grievous underlying malady of instability in m_H^2. The difference between the Higgs mass divergence (2.7) and other renormalizable divergences is that the others are only logarithmic. The quadratic form of the divergence (2.7) raises problems of naturalness [24]: if the cutoff $\Lambda > O(1)$ TeV^2 then the corrections δm_H^2 to the Higgs mass squared become larger than its physical value. On the other hand, logarithmically divergent loop corrections to other quantities such as fermion masses are numerically small even if $\Lambda >> O(1)$ TeV. Large corrections (2.7) to m_H^2 seem unnatural to many theorists, who therefore seek models with some effective cutoff $\Lambda = O(1)$ TeV.

Related difficulties arise whenever one tries to construct theories containing two or more very different mass scales, e.g. $m_W = m_H \times O(10^{\circ \pm 1})$ and the Planck mass $m_P \simeq O(10^{19})$ GeV or the grand unification scale $m_X \gtrsim O(10^{15})$ GeV. Hawking and collaborators [24] claim that elementary Higgs bosons propagating (fig.5b) through the space-time foam expected in the quantum gravitational vacuum acquire large mass shifts:

$$\delta m_H^2 = O(m_P^2) = O(10^{19}\text{GeV}) \tag{2.8}$$

Moreover, elementary Higgses propagating through a GUT vacuum acquire [25]

$$\delta m_H^2 = O(m_X^2) \gtrsim O(10^{15}\text{GeV})^2 \tag{2.9}$$

from their couplings to GUT Higgses with large vacuum expectation values $O(m_X) \gtrsim O(10^{15})$ GeV). Even if the large δm_H^2 (2.8, 2.9) are cancelled by some mechanism, radiative corrections involving transitions to heavy virtual particles with masses $O(m_X)$ can upset the delicate cancellation in m_H [25,26]. For example, loop corrections in GUT's give

$$\delta m_H^2 = O(\alpha^n m_X^2) \tag{2.10}$$

and some miracle should be found to cancel these loop corrections through $O(\alpha^{10} m_X^2)$! These examples illustrate the fact that it is difficult to construct theories with two or more vastly different mass scales, e.g. $m_W << m_X$ or m_P. The heavy scale tends to leak into the light scale via the Higgs. This is often termed the hierarchy problem: why is $m_W/m_P = O(10^{-17})$? One possible solution [20] to these instability problems is to dissolve the Higgs by making it a composite scalar bound state of new fermionic constituents called "technifermions" which have new "technicolour" interactions analogous to QCD, but becoming strong at a scale

$$\Lambda_{TC} = O(\frac{m_W}{\sqrt{\alpha}}) = O(1\text{ TeV}) \tag{2.11}$$

whereas QCD becomes strong at $\Lambda_C = O(1\text{ GeV})$. While it is easy to construct technicolour models giving masses to the $W^{\pm}$ and Z°, giving masses to quarks and leptons has proved to be much more difficult. Early prescriptions [27] for solving this problem involved extending the technicolour model in a way which predicted flavour-changing neutral interactions that

were too large [28], and light charged spin-zero bosons $P^{\pm}$ which should have been detected in experiments at PETRA and PEP [29]. Technicolour is therefore out of theoretical favour at the moment. However, it has never been demonstrated that a phenomenologically acceptable technicolour model cannot be constructed [30], so we retain technicolour as an interesting theory to test experimentally and as a yardstick for measuring the potential of a high energy hadron-hadron collider.

An alternative solution to the instability problems of elementary Higgses is to protect their masses and cancel out large loop corrections by invoking supersymmetry (susy). Several miraculous cancellations ocur in susy theories. The quadratic divergences due to bosons and fermions in fig.5a have positive and negative signs respectively. Therefore, if one has pairs of bosons and fermions with identical couplings available to circulate in the loops, as in a susy theory, one has

$$\delta m_H^2 = O(\alpha) \times |m_B^2 - m_F^2| \tag{2.12}$$

which can be less than the $O(m_W^2)$ required for m_H^2 by perturbative unitarity if

$$|m_B^2 - m_F^2| \gtrsim O(1)\ \text{TeV}^2 \tag{2.13}$$

corresponding to a low effective cutoff: $\Lambda^2 = O(1)\ \text{TeV}^2$. A second miracle is the absence of large Δm_H^2 from propagation through space-time foam in a susy theory. Finally, if the GUT contribution (2.9) to m_H is cancelled in a susy theory, no contributions of the form (2.10) are generated by radiative corrections. This is thanks to certain miraculous no-renormalization theorems [32] in susy theories which guarantee that many logarithmic divergences are absent. Because of these miracles, m_H is stabilized in a susy theory, and therefore m_W is also stabilized against the effects of radiative corrections. However, there is no fundamental understanding of the origin of the weak interaction scale, which means that the hierarchy problem is not really solved by susy. But at least some technical progress is made in alleviating the symptoms of the disease.

2.4 Supersymmetric Particles and their Signatures

Cancelling the unwanted loop diagrams required bosons and fermions with identical couplings and similar masses. These are provided in susy theories which contain particles in the following supermultiplets [33]:

$$\text{gauge: } \begin{pmatrix} 1 \\ 1/2 \end{pmatrix}, \quad \text{chiral: } \begin{pmatrix} 1/2 \\ 0 \end{pmatrix} \tag{2.14}$$

Unfortunately, no known particle is the spartner of any other known particle, which requires a doubling of the elementary spectrum and the invention of many new names as seen in Table 1.

Table 1: Supersymmetric Spectrum

particle	spin	sparticle	spin
quark $q_{L,R}$	$\frac{1}{2}$, $\frac{1}{2}$	squark $\tilde{q}_{L,R}$	0, 0
lepton $l_{L,R}$	$\frac{1}{2}$, $\frac{1}{2}$	slepton $\tilde{l}_{L,R}$	0, 0
photon γ	1	photino $\tilde{\gamma}$	$\frac{1}{2}$
gluon g	1	gluino $\tilde{g}$	$\frac{1}{2}$
$W^{\pm}$	1	wino $\tilde{W}^{\pm}$	$\frac{1}{2}$
Z°	1	zino $\tilde{Z}^{\circ}$	$\frac{1}{2}$
Higgs $H^{\circ,\pm}$	0	shiggs $\tilde{H}^{\circ,\pm}$	$\frac{1}{2}$

The absence [29] of any charged sparticle at PETRA and PEP means that

$$m_{\tilde{q}},\ m_{\tilde{l}},\ m_{\tilde{W}^{\pm}},\ m_{\tilde{H}^{\pm}} \gtrsim O(20)\ \text{GeV} \tag{2.15}$$

The absence of a signal in SPS and FNAL beam dump experiments [34] mean that coloured sparticles must be massive and in particular

$$m_{\tilde{g}} \gtrsim O(3)\ \text{GeV} \tag{2.16}$$

with the precise value dependent on the assumed squark mass. Experiments [4] at the CERN $p\bar{p}$ Collider can be used [35] to argue that

$$m_{\tilde{g},\tilde{q}} \gtrsim O(40)\ \text{GeV} \tag{2.17}$$

There is no particle physics bound on colourless neutral sparticles, but cosmology [36] suggests that the lightest sneutral may be the photino, and

$$m_{\tilde{\gamma}} \gtrsim O(\tfrac{1}{2})\ \text{GeV} \tag{2.18}$$

with the precise value dependent on the assumed masses of sleptons and squarks.

The fact that in general particles and sparticles have different masses means that supersymmetry must be broken, just as $m_K \neq m_\pi$ means that flavour SU(3) had to be broken. It may well be that supersymmetry is broken spontaneously, as we believe to be the case with electroweak gauge symmetry. The precise mechanism of supersymmetry breaking need not

concern us here: many models [37] with broken supersymmetry also have the desired miraculous cancellations. By how much can supersymmetry be broken? or in other words, how heavy could the unseen sparticles be? In supersymmetric theories the self-couplings of the Higgs particles are specified to be $O(\alpha)$, and the masses of the Higgs bosons are fixed to be close to $m_{W^\pm}$ and m_{Z°. Therefore we expect from equation (2.13) that the sparticles will have masses below $O(m_W/\sqrt{\alpha}) = 1$ TeV, and this is indeed the case in most though not all models [37].

In most models [37] there is an exactly conserved multiplicative quantum number R = +1 for ordinary particles and R = -1 for sparticles. This means that sparticles can only be produced in pairs, that their decay products always contain another sparticle, and hence that the lightest sparticle is absolutely stable. In this case cosmology probably requires the lightest sparticle to be neutral and not strongly interacting, as was assumed in deriving the limit (2.18). In models where R-parity is conserved the signature of susy is missing energy-momentum carried off by the missing sneutral, probably [36] the photino:

$$\tilde{q} \to q + \tilde{\gamma}, \quad \tilde{l} \to l + \tilde{\gamma}, \quad \tilde{g} \to q\bar{q}\,\tilde{\gamma} \tag{2.19}$$

These are the susy signatures developed most extensively in section 3. However, it is possible to construct models [38] in which R-parity is violated in which case sparticles may decay into leptons such as the τ or the ν_τ:

$$\tilde{q} \to q + \begin{pmatrix} \nu_\tau \\ \tau \end{pmatrix} \quad , \quad \tilde{l} \to l + \begin{pmatrix} \nu_\tau \\ \tau \end{pmatrix} \quad , \gamma \to \begin{pmatrix} \nu_\tau \\ \tau \end{pmatrix} + e\begin{pmatrix} e \\ \nu \end{pmatrix} \tag{2.20}$$

This alternative is also discussed in section 3.

Sparticle masses are very model-dependent, but typically $<O(1)$ TeV because of the cancellation argument (2.13). As discussed in more detail in section 3, rates [39] for the production at high-energy hadron colliders with $\sqrt{s} = O(20)$ TeV of coloured sparticles, q and $\tilde{g}$, are large enough for $m_{\tilde{g},\tilde{q}} \gtrsim O(1)$ TeV to be detected. There are no obvious physics backgrounds to the missing transverse energy signatures provided by the canonical decay patterns (2.19). While a detailed evaluation of instrumental backgrounds is not included in our brief [40], we do not believe that they are very troublesome. Therefore, as we will see in more detail in section 3, looking for heavy sparticles in high energy hadron-hadron collisions will be relatively easy.

2.5 The Technicolour Alternative

We also study in section 3 what the phenomenology of a realistic technicolour theory[20,41] might resemble. We assume that a realistic theory contains [41] a complete new technigeneration of fermions: $(U_{R,Y,B}; D_{R,Y,B}, E, N)$. Since such a theory has a whole new set of strong interactions on a scale $\Lambda_{TC} = O(1)$ TeV (2.11), one expects [41] a rich spectroscopy of new states with masses in this range:

$$\text{techni}\rho : m_{\rho_T} = O(1) \text{ TeV} , \quad \text{technibaryon} : m_{B_T} = O(1) \text{ TeV, etc.} \tag{2.21}$$

as illustrated in Table 2. Also shown in Table 2 are the many "low-mass" technipions with masses $\ll$ 1 TeV which are anticipated in extended technicolour models which seek to understand quark and lepton masses. As already mentioned, all existing technicolour models are unsatisfactory, in part because the $P^{\pm}$ of Table 2 have not been discovered [29], and it may be that Table 2 is not a reliable guide to technispectroscopy. Nevertheless, it is the best we have. Of particular interest in high-energy hadron-hadron collisions are the colour octet states P_8 , ρ_8 etc. One would expect the decay signatures

$$P_8^0 \to \bar{t}t,\ P_8^{\pm} \to g + W^{\pm}\ ,\ \rho_8, \omega_8 \to \text{technipions} \qquad (2.22)$$

Rates for production of P_8, ρ_8 and the technifermion continuum are large at $\sqrt{s}$ = O(20) TeV, and the signatures (2.22) are probably detectable as we will see in more detail in section 3.

Table 2: Technihadron masses

	Particle	Description	Mass
Technipions	P^0,	e.m. neutral color singlet	$\leq$ 3 GeV ?
	$P^{\pm}$	e.m. charged color singlet	$\leq$ 15 GeV ?
	P_{LQ}	leptoquarks color triplet	150 GeV
	$P_8^{0,\pm}$	color octet	250 GeV
	ρ_T	color singlet octet	$\sqrt{4/N_{TC}}$ x 900 GeV
	ω_T	color singlet octet	$\sqrt{4/N_{TC}}$ x 900 GeV
	η_T'	e.m. neutral color singlet	$\sqrt{4/N_{TC}}$ x 970 GeV
	f_T,etc	color singlet, octet	$\sqrt{4/N_{TC}}$ x 1500 GeV, etc.
	B_T	technibaryons	$\sqrt{N_{TC}/4}$ x 1500 GeV

The number of technicolours is denoted by N_{TC}.

3 - Production and Detection of New Particles

3.1 - General Comments on Rates and Distributions

We have seen in section 2 that extant models of gauge symmetry breaking (elementary Higgs bosons, supersymmetry, technicolour) all firmly expect some new physics in the 1 TeV range. The new particles that these models predict are the main foci of our studies in this section. Before getting into details, we first make a few general remarks for orientation purposes.

If the mass of a new particle system x is quite heavy ($m_x >> 1$ GeV), and if its ratio to the total centre-of-mass energy is not too low ($m_x/\sqrt{s} \quad O(10^{-2})$?), its production cross-section at a hadron-hadron collider can be estimated quite reliably (to within a factor of a few ?) using the model illustrated in fig.6. The general approximate form of the cross-section is given by the Drell-Yan [42] formula:

$$\sigma(x) = \sum_{a,b} \int d\tau \; L_{ab}(\tau) \; \hat{\sigma}_{ab}(x) \tag{3.1}$$

where $\hat{\sigma}$ is the cross-section for a parton-parton subprocess a + b → x, e.g.

$$\hat{\sigma}_{q\bar{q} \to \gamma^* \to L^+L^-} = \frac{4\pi\alpha^2 e_q^2}{9m_x^2} \beta(3 - 2\beta^2): \beta = \sqrt{(1 - \frac{4m_L^2}{m_x^2})}$$

for heavy-lepton pair production via a virtual photon of invariant mass m_x, and $L_{ab}(\tau)$ is the parton-parton luminosity function for ab collisions:

$$L_{ab}(\tau) = \int dx_a \int dx_b a(x_a) b(x_b) \delta(x_a x_b - \tau) \tag{3.3}$$

where

$$\tau = x_a x_b \equiv m_x^2/s : x_a = 2p_a/\sqrt{s} \; , \; x_b = 2p_b/\sqrt{s} \quad , \quad \sqrt{s} = E_{cm} \tag{3.4}$$

The parton fractional momentum distributions $a(x_a)$ etc. should be evaluated at some momentum scale $Q = O(m_x)$, evolved from lower scales using the QCD Altarelli-Parisi equations [43]. The formalism (3.1, 3.2, 3.3) predicts correctly to within a factor of 2 the cross-sections for production of lepton pairs with $m_x > 4$ GeV in fixed target experiments and $m_x \approx m_{W^\pm}$ or m_{Z^0} in collider experiments [1,2]. The discrepancies between experiment and the naive theory (3.1) have the same sign and order of magnitude as the computed higher order QCD corrections to equation (3.1), though these corrections are O(1) and difficult to estimate quantitatively. The same formalism (3.1, 3.2, 3.3) is applicable [44] to large p_T strong interaction cross-sections, and seems to work there also to within a factor of 2. Not all the next-to-leading order QCD contributions to large p_T jet production have yet been calculated.

Generically, one expects subprocess cross-sections to have geometrical values characteristic of the collisions of point-like particles:

$$\hat{\sigma}(m_x) \approx \frac{1}{m_x^2} \times \begin{cases} O(10^{-4}) & \text{for electroweak processes} \quad (3.5a) \\ O(1) & \text{for strong processes} \quad (3.5b) \end{cases}$$

The Drell-Yan subprocess cross-section (3.2) exemplifies the general rule (3.5a). The rule (3.5b) is an effective upper bound on the possible cross-section for the point-like production of new particles. It tells us that even though a very high energy hadron-hadron collider offers in principle the possibility of parton-parton collisions at m_X up to $\sqrt{s}$, in practice the collision rates will be bounded above by the luminosity functions $L_{ab}(\tau)$ (3.3), which are known to fall monotonically with increasing τ. The precise forms of all the parton-parton luminosity functions are not well determined in fixed target experiments at $Q^2 \leq O(100)$ GeV^2. For example, it is difficult to measure parton distributions at $x \leq O(10^{-2})$, and gluon distributions may only be determined indirectly in lepton-hadron collisions, with the result that their shapes are strongly correlated with the fitted value of the QCD scale parameter Λ. However, these uncertainties tend to wash out at very large $\sqrt{s}$ and m_X, although it is always difficult to make reliable predictions for parton distributions at $x \leq O(10^{-2})$. Even if one knew precisely the low energy input structure functions, the logarithmic QCD extrapolation to higher energies is more uncertain here than at larger values of x. Shown in fig.7 are some of the effective parton- parton luminosity functions that we use in our cross-section calculations. They are obtained [45] from CDHS structure functions [46] evolved up to the appropriate energies using the Altarelli-Parisi equations [43]. Comparisons with other calculations [47] lead us to believe that our parton-parton luminosities are not likely to mislead by more that a factor of 2 for $x \gtrsim O(10^{-2})$, which is in any case within the inevitable range of uncertainty due to higher order corrections. We see from fig.7 that because of the general rules (3.5), one is unlikely to have observable cross-sections for new strongly interacting particles which weigh more than a few TeV, even if the available centre-of-mass energy is an order of magnitude higher.

When comparing machines with different centre-of-mass energies but the same hadron-hadron luminosity, the geometrical factors of $1/m_X^2$ (3.5) imply that any given parton-parton subprocess has an observably large cross-section only up to values of τ which decrease as $\sqrt{s}$ increases. One must compensate for the lower values of $\hat{\sigma}$ by going to lower values of τ where $L(\tau)$ is larger (fig.7). This effect is seen in fig.8, where we have plotted the luminosity (3.3) multiplied by the geometric factor $1/m_X^2$ (3.5). The horizontal axis is taken to be m_X, the vertical axis has the dimensions of a cross-section, and we have included horizontal lines corresponding to plausible limits of observability for hadron-hadron colliders with liminosities in the range 10^{32} to 10^{33}cm^{-2}sec^{-1}. The curves plotted are for gg and $u\bar{u}$ luminosities in pp and $p\bar{p}$ collisions at $\sqrt{s}$ = 10, 20 and 40 TeV.

As a rule of thumb in the region of interest, the effective range of m_X in which one can probe for new physics increases like

$$m_X \propto (\sqrt{s})^{0(\frac{1}{2})} \tag{3.6}$$

It is easy to see from fig.7 how one loses physics reach at fixed $\sqrt{s}$ if one decreases the available hadron-hadron luminosity L. As a rule of thumb in the region of interest, the effective range of m_X in which one can probe for new physics decreases like

$$m_X \propto L^{0(0\cdot2)} \tag{3.7}$$

The first rule (3.6) must be borne in mind when considering possible values of $\sqrt{s}$ (10, 20 or 40 TeV?), and the second rule (3.7) must be borne in mind when considering the relative merits of pp and $\bar{p}p$ colliders.

It seems likely that $p\bar{p}$ colliders will be limited to luminosities at least one order of magnitude smaller than pp colliders, say $10^{32}cm^{-2}sec^{-1}$ for $p\bar{p}$ rather than $10^{33}cm^{-2}sec^{-1}$ for pp. Comparing figs.8a and 8b, one then sees that the physics reaches for producing strongly interacting particles by $u\bar{u}$ collisions, as indicated by the horizontal "limits of observability" lines, are very similar for pp and $p\bar{p}$ colliders having the same $\sqrt{s}$. The assumed factor of 10 advantage in hadron-hadron luminosity of a pp machine is essentially cancelled by the $p\bar{p}$ advantage in parton-parton luminosity at large values of τ: compare the dotted horizontal line in fig.8a with the dashed horizontal line in fig.8b. On the other hand, it is clear from fig.8c that one loses physics reach for particle production by gg collisions if one decreases the hadron-hadron luminosity by a factor 10, as expected when comparing pp and $p\bar{p}$ collisions. Moreover, the pp advantage in hadron-hadron luminosity is also significant when considering a electroweak production mechanism. In such a case the subprocess cross-section $\hat{\sigma}$ (3.5a) is likely to be $O(10^{-4})$ of a strong cross-section at the same invariant mass. This means that the "limit of observability" occurs at a much lower value of τ, where the difference between the $u\bar{u}$ parton-parton luminosities in pp and $p\bar{p}$ collisions is much less significant. Thus pp colliders with a hadron-hadron luminosity of $10^{32}cm^{-2}sec^{-1}$ generally give more events than $p\bar{p}$ colliders of the same $\sqrt{s}$ with a hadron-hadron luminosity of $10^{32}cm^{-2}sec^{-1}$, with the limited exception of the production of very high mass strongly interacting particles via $u\bar{u}$ collisions. In most of the range of interest, luminosity functions in pp and $p\bar{p}$ collisions do not differ by more than a factor of 2, which therefore accords no great physics advantage to $p\bar{p}$ collisions. Indeed, the differences between the pp and $p\bar{p}$ cross-sections are typically smaller than the likely theoretical errors in estimating the absolute values of these cross-sections. Nevertheless, in what follows we always state whether a given cross-section is calculated for a $p\bar{p}$ or a pp collider.

Heavier particles which are produced with smaller cross-sections closer to the limit of observability are produced predominantly centrally, with rapidity $|y| = O(1)$. For example, Higgses of 200 GeV produced in association with a $t\bar{t}$ pair (see section 3.2) have $\langle y^2\rangle^{\frac{1}{2}} = 1{\cdot}1$, while the q and $\bar{q}$ jets coming from pair-production of gluons weighing 1 TeV (see section 3.3) have $\langle y^2\rangle^{\frac{1}{2}} = 1{\cdot}2$. By contrast, particles of smaller mass, which are generally produced with larger cross-sections, generally tend to be produced closer to the beam directions. For example, it has been estimated [49] that at $\sqrt{s} = 40$ TeV $W^{\pm}$ are produced in the rapidity range $|y| < O(5)$, with 2/3 going within 5° of the beam-pipes (fig.9). These are specific examples of an analogy between production angles and the depths of sedimentary strata in which archeologists search for ancient artefacts, illustrated in fig.10. At any given accelerator, the new physics of the day tends to be produced at large angles, while yesterday's physics is produced closer to the beams, and last week's physics passes down the beam pipes. At present, today's new physics is the $W^{\pm}$, Z° and hadron jets with $p_T = O(100)$ GeV, all of which are currently produced at large angles. However, at the LHC the $W^{\pm}$ and Z° will be swept forward and backward in the centre-of-mass, as we have seen. We hope they will be replaced at large angles by gluinos or Higgses or?

In addition to the single-subprocess hard scattering cross-sections given by (3.1), there can also be events featuring two hard parton-parton collisions [22] in parallel, as illustrated in fig.11. As we will see later in Section 3, some of such multiple hard collisions could provide significant backgrounds to new particle searches. To estimate these double cross-sections, one needs two-parton distributions

$$a(x_{a_1}, x_{a_2}) \tag{3.8}$$

which are not known in general, although some model distributions have been proposed [50]. The double distributions (3.8) do not in general factorize, but model studies [22] indicate that factorization gives an approximation to the double subprocess total cross-section which may be correct to within a factor of order 2, if one is considering processes initiated by partons with low values of x. In what follows we therefore estimate these double subprocess cross-sections by

$$\sigma(x_1, x_2) = \left(\frac{\sigma(x_1)}{\sigma_{tot}}\right) \left(\frac{\sigma(x_2)}{\sigma_{tot}}\right) \times \sigma_{tot} \tag{3.9}$$

where σ_{tot} is the total pp cross-section $\approx$ 100 mb.

3.2 - Higgs production and signatures

We consider several mechanism for Higgs production at hadron colliders in sections 3.2.1 to 3.2.5, as well as several sources of physics background in section 3.2.6.

3.2.1 - gg → H

This reaction proceeds via virtual quark diagrams as shown in fig.12. The total cross-section is

$$\sigma_{gg\to H} = \frac{\sqrt{2}\, G_F}{64} \frac{\alpha_s^2}{\pi} \frac{|N|^2}{9} \tau \frac{dL_{gg}}{d\tau} \tag{3.10}$$

where $N = \Sigma_q N_q$:

$$N_q = 3[2\lambda_q + \lambda_q(4\lambda_q - 1)f(\lambda_q)] \tag{3.11a}$$

with

$$\lambda_q \equiv m_q^2/m_H^2 \,, \quad f(\lambda_q) = \begin{cases} -2\left(\sin^{-1}\frac{1}{2\sqrt{\lambda_q}}\right)^2 & \text{for } \lambda_q > \frac{1}{4} \\ \frac{1}{2}\log\left(\frac{\eta^+}{\eta^-}\right) - \frac{\pi}{2} + i\pi \log\left(\frac{\eta^+}{\eta^-}\right) & \text{for } \lambda_q < \frac{1}{4} \end{cases} \tag{3.11b}$$

and

$$\eta^{\pm} \equiv \frac{1}{2} \pm \frac{1}{4} - \lambda \tag{3.11c}$$

Total cross-sections (no rapidity cuts) are shown in fig.13 for $\sqrt{s}$ = 10, 20, 40 TeV, m_t = 35, 70 or 100 GeV and a range of Higgs masses between 200 GeV and 1 TeV.

The cross-sections can only be estimated approximately when m_H O(200) GeV. The cross-sections depend sensitively on the assumed masses of the quarks propagating round the loops, with

$$|N|^2 \begin{cases} = O(m_q^4/m_H^4 \ln (m_q^2/m_H^2)) \text{ as } m_q/m_H \to 0 \\ \to 1 \quad \text{as } m_q/m_H \to \infty \end{cases} \tag{3.12}$$

We have only included one heavy quark in calculating fig.13, which we take to be the t quark, though there could be important contributions from representatives of a fourth generation. In fig.13 we have taken m_t = 35, 70 and 100 GeV: the cross-sections increase rapidly with m_t as long as $m_t \ll m_H$, quantitatively as one expects from equation (3.12), although the analytic form 3.12 is not a good approximation throughout the interesting range of m_t. Even if the t quark were soon found to have a mass O(35) GeV, the cross-section for gg → H could be substantially increased if there is a fourth generation. The rapidity distribution of the Higgs decay products is shown in fig.14 for different values of m_H. - We see that, as expected, the rapidity distribution is more central for larger m_H. The Higgs will decay isotropically in into centre-of-mass frame, predominantly into $\bar{t}t$ if $2m_t < m_H < 2m_W$, and into W^+W^- or $Z^\circ Z^\circ$ for $m_H > 2m_W$. Possible backgrounds are considered in section 3.2.5.

3.2.2 - $\bar{q}q \to H$, $g + q \to q + H$

It is necessary to distinguish two contributions of this sort to Higgs production: via the annihilation of light quarks which are copions inside nucleous, and via heavy quarks which are rare. The coupling (2·1) of the standard model Higgs to ligh quarks is so small α m_q: $m_{u,d} \approx 10$ MeV, $m_s \approx 200$MeV) that they make a negligible contribution to Higgs production [15]. The dominant perturbative QCD contribution to Higgs production via heavy quarks is likely to be that discussed in the next subsection. However, it is a priori possible that there might be an important nonperturbative contribution due to an "intrinsic" component of heavy quarks in the proton. The existence of such an intrinsic heavy quark component has been proposed [52] in connection with the diffractive production of charm, and similar diffractive production of the t quark, due to "intrinsic top" in the proton, is now being looked for at the CERN $p\bar{p}$ Collider. The existence of an "intrinsic" charm component at the proposed [52] level does not [53] conflict with EMC data [54] on dimuon production. Production of light Higgs at lower energies via intrinsic charm has already been considered [55]. It is easy to scale the cross-sections found there up to higher $\sqrt{s}$ using the t quark - Higgs coupling αm_t instead of α m_c:

$$d\sigma|_t \; / \; d\sigma|_c = O(\frac{m_c^2}{m_t^2}) \times (\sqrt{s}|c \; / \; \sqrt{s}|t \;)^2 \tag{3.13a}$$

for similar values of $m_H/\sqrt{s}$ and of the kinematic variables such as the rapidity y. In deriving the ratio (3.13) we have assumed similar distributions for intrinsic charm and intrinsic top, but scaled [52] by $O(1/m_q^2)$ in each of the two colliding nucleons. Using

equation (3.13) to compare H production at a collider with $\sqrt{s}$ = 10 to 20 TeV with lighter Higgs production at $\sqrt{s}$ = 10 to 20 GeV, we find a suppression factor of order 10^{-5}. Since previously quoted cross-sections for low $\sqrt{s}$ collisions were at most $O(10^{-38}\,cm^2)$ this suggests that intrinsic $\bar{t}t$ annihilation would not make a significant contribution to H production at the colliders of interest to us here.

Potentially more interesting might be bremsstrahlung of Higgs from an "intrinsic" heavy quark struck by a gluon: e.g. $g + t \to H + t$ [56]. Assuming intrinsic distributions independent of m_q apart from an overall normalization factor $O(1/m_q^2)$, this cross-section scales as

$$d\sigma|_t / d\sigma|_c = O(\frac{m_c^2}{m_t^2}) \qquad (3.13b)$$

for similar values of y, m_q/m_H and $m_H/\sqrt{s}$. Scaling from m_H = 10 GeV, $\sqrt{s}$ = 800 GeV and m_c = 1·5 GeV to m_H = 250 GeV, $\sqrt{s}$ = 20 TeV and $m_t \approx$ 38 GeV, the low-energy calculations of ref.56 yield an estimate of 10^{-3} pb. While giving a cross-section considerably larger than the $\bar{t}t$ annihilation mechanism estimated previously, this $g + t \to H + t$ mechanism does not seem to be competitive in terms of rate and event signature with other mechanisms. Therefore we have not studied it further.

3.2.3 - $\bar{q}q$ or $gg \to \bar{t}tH$

The underlying mechanism in these reactions is Higgs bremsstrahlung from a heavy quark as in fig.15. The subprocess cross-section for $\bar{q}q \to \bar{t}tH$ is known[57] in analytic form:

$$\hat{\sigma}(\bar{q}q \to \bar{t}tH) = \frac{\alpha_s^2 G_F m_t^2}{36\sqrt{2}\pi^2 s^2} \int \frac{d^3k_{\bar{t}}}{2k^\circ_{\bar{t}}} \int \frac{d^3k_e}{2k^\circ_t} \int \frac{d^3k_h}{2k^\circ_h} \delta^4(p_q + p_{\bar{q}} - k_t - k_{\bar{t}} - k) |M|^2 \qquad (3.14a)$$

where

$$|M|^2 = \frac{32}{(2k_h\cdot k_{\bar{t}} + m_H)(2k_h\cdot k_t + m_H)} \{(p_q+p_q)^2((p_q+p_{\bar{q}})\cdot p)^2[1 + \frac{(4m_t^2 - m_H^2)(p_q + p_{\bar{q}})^2}{(2k_h\cdot k_t + m_H^2)(2k_h\cdot k_{\bar{t}} + m_H^2)}] \qquad (3.14b)$$

$$+ [((p_q+p_{\bar{q}})^2 + m_H^2 - 4m_t^2) + \frac{2(p_q+p_{\bar{q}})\cdot k_h (4m_t^2 - m_H^2)}{(2k_h\cdot k_{\bar{t}} + m_H^2)}][\frac{(p_q+p_{\bar{q}})^2}{2} m_t^2 - 2(k_t\cdot p_q)(p_{\bar{q}}\cdot k_t)]$$

$$+ (k_t \leftrightarrow k_{\bar{t}}) - ((p_q+p_{\bar{q}})^2 + m_H^2 - 4m_t^2)\,[2(k_t\cdot p_q)(k_{\bar{t}}\cdot p_{\bar{q}}) + 2(k_t\cdot p_{\bar{q}})(k_{\bar{t}}\cdot p_q) - (p_q+p_{\bar{q}})^2(k_t\cdot k_{\bar{t}})]\}$$

The evaluation of $gg \to \bar{t}tH$ involves the interferences between several different diagrams obtained by permuting the external gluons and coupling the H to the different internal and external t quark lines. No complete analytic calculation is available, but we have used the outputs of 2 different algebraic programs [57,58] for the trace calculation. Results for m_t = 35 GeV and different choices of m_H and $\sqrt{s}$ are shown in fig.16. We have not been able to confirm the large cross-sections or the shapes of the Higgs rapidity distributions reported in ref.57. Some final state distributions for a representative m_H = 200 GeV and $\sqrt{s}$ = 20 TeV are shown in fig.17. Fig.17a gives the rapidity distribution of the Higgs, and fig.17b that of the accompanying t (or $\bar{t}$) quark. Fig.17c shows the p_T distribution of the Higgs, while fig.17d shows that of the accompanying t (or $\bar{t}$) quark. Finally, fig.17e show

the distribution in invariant mass of the spectator ($\bar{t}t$) system. We see that the Higgs is produced quite centrally, as previously advertized, and with an average p_T = O(100) GeV. The additional event signature of a spectator ($\bar{t}t$) pair in the final state may be used to reduce the backgrounds below those encountered in gg H production.

3.2.4 - WW → H

This process [59] is an electroweak analogue of $\gamma\gamma$ scattering in e^+e^- annihilation, as seen in fig.18. The subprocess cross-sections for $ud \to duH$, $u\bar{u} \to u\bar{u}H$, $d\bar{d} \to d\bar{d}H$, $\bar{u}\bar{d} \to \bar{u}\bar{d}H$ and analogous processes involving strange quarks are all identical: the matrix elements squared are

$$|M|^2 = 64 g_{VVH}^2 \left[\frac{C_1(p_1 p_2)(p'_1 p'_2) + C_2(p_1 p'_2)(p'_1 p_2)}{(q_1^2 - m_V^2)^2 \; (q_2^2 - m_V^2)^2} \right. \tag{3.15a}$$

In the expression (3.14b)

$$g_{VVH} = \begin{cases} g \cdot m_W & \text{for } WW \to H \\ g \cdot \dfrac{m_Z}{\cos\theta_W} & \text{for } ZZ \to H \end{cases} \tag{3.15b}$$

and

$$C_1 = g_L^2 g_L'^2 + g_R^2 g_R'^2 \;, \quad C_2 = g_L^2 g_R'^2 + g_R^2 g_L'^2 \tag{3.15c}$$

where

$$g_{L,R} = \frac{1}{2}(g \mp g_A) \tag{3.15d}$$

with

$$\left.\begin{aligned} g_V &= -g_A = \frac{g}{2\sqrt{2}} \qquad \text{for } W^{\pm} \\ g_V &= \frac{g}{\cos\theta_W} \left(\tfrac{1}{2} T_{3L} - Q \sin^2\theta_W\right) \\ g_A &= -\frac{g}{\cos\theta_W} \left(\tfrac{1}{2} T_{3L}\right) \end{aligned}\right\} \text{for } Z^\circ \tag{3.15e}$$

An approximate form for the subprocess cross-section (3.14a), integrating after all the final state variables, is:

$$\hat{\sigma}(qq \to qqH \text{ via } WW) = \frac{1}{16\sqrt{6} m_W} \left(\frac{\alpha}{\sin^2\theta_W}\right)^3 \log\left(\frac{\hat{s}}{m_H^2}\right) \tag{3.16}$$

The total cross-section for WW → H in $p\bar{p}$ collisions is shown in fig.19 for interesting ranges of m_H and $\sqrt{s}$. We see that the cross-sections are larger than those for gg → H when m_H > O(500) GeV. Unfortunately, when it is so heavy the Higgs is so wide that it may be difficult to pick out from the WW or Z°Z° continuum. The vector boson poles in (3.14a) tend to give sharp forward-backward peaking for the final state q (or $\bar{q}$) and a flat rapidity distribution for the Higgs (hence the logarithm in equation (3.16). It is possible to compute [60] analytically from equations (3.15) the form of the Higgs distribution in the centre-of-mass frame of the parton-parton subprocess. It exhibits

strong forward-backward peaking when $\hat{s} >> m_H^2$:

$$\frac{d^2\hat{\sigma}}{d\cos\hat{\theta}}_{\sqrt{\hat{s}}>>m_W} = \frac{4C_1 g_{\nu\nu H}^2}{\pi^3 \hat{s}^2} \left(\frac{\pi^2}{3} - \frac{13}{4}\right)\left(\frac{\sqrt{\hat{s}}}{2m_W}\right)^6 \qquad (3.17)$$

reflecting the kinematical similarity of this process to $\gamma\gamma$ scattering. The rapidity distribution [60] of the Higgs in the parton-parton subprocess centre-of-mass is shown in fig.20. Because of the peaking (3.17) the scattered quarks or antiquarks in the final state do not get out to large enough p_T to provide a distinctive signature, such as was provided by the $(\bar{t}t)$ pair in the previous reaction.

3.2.5 - $\bar{q}q \to W^{\pm *} \to W + H$

The diagram for this subprocess is shown in fig.21. The subprocess cross-section for $\bar{q}q \to (W^{\pm *}$ or $Z^{o*}) \to (W$ or $Z^o) + H$ is [19,61]

$$\sigma_{VH} = \frac{g_{VVH}^2}{24\pi} \frac{g_V^2 + g_A^2}{(\hat{s}-m_V^2)^2} \frac{p_V}{\sqrt{\hat{s}}} \left(1 + \frac{p_V^2}{3m_V^2}\right) \qquad (3.18a)$$

where g_{VVH}, g_V and g_A were introduced in (3.15), and p_V is the final state momentum of the H in the subprocess centre-of-mass:

$$p_V = \frac{(\hat{s}^2 + m_V^4 + m_H^4 - 2\hat{s}m_V^2 - 2\hat{s}m_H^2 - 2m_V^2 m_H^2)^{\frac{1}{2}}}{2\sqrt{\hat{s}}} \qquad (3.18b)$$

The total cross-section for these processes is not very large, falling below the limit(?) of observability of 1/10 pb for m_H = O(200 to 400) GeV, as seen in fig.22. This process has the distinctive final state event signature of 3 intermediate vector bosons if $m_H > 2m_W$. Unfortunately, the fall-off of the cross-section curves in fig.22 means the total cross-section is probably unolservably small in the region of large m_H (>400 GeV) where its natural width is too large for it to appear as a sharp resonance above the WW continuum.

3.2.6 - Observability

As stated in section 2, we assume that any Higgs with mass less than about 100 GeV will have been detected by LEP [21] before this large hadron-hadron collider starts operation. A compilation of cross-sections for heavy Higgs production in $p\bar{p}$ collisions at $\sqrt{s}$ = 20 TeV is shown in fig.23. Cross-sections for 100 GeV < m_H < 200 GeV are tricky to estimate because there we get into regions of $\sqrt{\tau} = \sqrt{x_1 x_2} \lesssim O(10^{-2})$ where we no longer have great confidence in the perturbative QCD extrapolation of the presently known parton distributions and the subprocess luminosity functions of fig.7. If 100 GeV < m_H < $2m_W$, we presume the dominant decay mode is $H \to \bar{t}t$. In this mass range , the largest production cross-section is that for $gg \to H$, but in this case the absence of any other final state event signature leaves us prey to the relatively large gg or $q\bar{q} \to \bar{t}t$ background shown in fig.24. If one assumes a plausible (?) mass resolution for $(\bar{t}t)$ pairs of order 10%, the $(\bar{t}t)$ background overwhelms the H signal. One could hope that the situation would be better if one looks for processes with final state event signatures such as gg or $\bar{q}q \to H\bar{t}t$ or

$q\bar{q} \to W+H$. For the $H\bar{t}t$ case we have estimated the background in two different ways. One uses a perturbative QCD calculation [58] of the 2 to 4 subprocesses giving $\bar{t}t\bar{t}t$ final states. The cross-section for this raction is estimated to be very large (fig.25) and overwhelms the $\bar{t}t+(H \to \bar{t}t)$ signal. We have tried unsuccessfully to get out the signal by implementing cuts on $p_T(H)$ or $p_T(t)$ or $m(\bar{t}t)$. Unfortunately, the final state distributions for $(\bar{t}t\bar{t}t)$ production shown in fig.26 are very similar to those for $(t\bar{t}+H)$ production in fig.17. The background from the double-subprocess mechanism (gg or $\bar{q}q \to \bar{t}t$)(gg or $\bar{q}q \to \bar{t}t$) estimated using the Ansatz (3.9) is much smaller than that due to the 2 to 4 subprocess (see Table 3) and would by itself be menageable. Turning to the process $\bar{q}q \to W+(H \to \bar{t}t)$, the backgrounds come from 2 to 3 reactions $\bar{q}q \to W\bar{t}t$ and from the double-subprocess reaction $(\bar{q}q \to W)$(gg or $\bar{q}q \to \bar{t}t$). A recent calculation [58] of the cross-section for $u\bar{d} \to W^+ + \bar{t}t$ indicates that it is not uncontrollably larger than that for $u\bar{d} \to W^{*+} \to W^+ + H$. Taking $\sqrt{\hat{s}}$=400GeV, m_W = 80 GeV and m_H = 120 GeV one has $\hat{\sigma}(u\bar{d} \to W+H) \approx 7 \times 10^{-2}$ pb, whereas the total subprocess cross-section for $u\bar{d} \to W^+ + \bar{t}t$ is $\hat{\sigma}(u\bar{d} \to W+\bar{t}t) \approx 1{\cdot}3$ pb. However, if one assumes a 10% resolution so that one can take the background in a bin of width $\Delta m(\bar{t}t) = \pm 5\%$ of $m(\bar{t}t) \approx 120$ GeV, one only has to contend with $\Delta\hat{\sigma} = d\hat{\sigma}/dm(\bar{t}t) \times \Delta m(\bar{t}t) \approx 7{\cdot}5 \times 10^{-2}$ pb. This ratio of signal tophysics background $\hat{\sigma}(W+H)/\Delta\hat{\sigma}(W+\bar{t}t) \approx 1$ to 1 does not vary strongly with either $\hat{s}$ or m_H. The background from the double-subprocess reaction $(\bar{q}q \to W)$ (gg or $\bar{q}q \to \bar{t}t$) seems to be manageably small, as seen in Table. 3.

Table 3: Double-subprocess backgrounds to Higgs searches at $\sqrt{s}$ = 20 GeV

Process	Signal cross-section (pb)	Background process	Background cross-section (pb)
$\bar{t}t+(H \to \bar{t}t)_{120GeV}$	3·6	(gg or $\bar{q}q \to \bar{t}t$)(gg or $\bar{q}q \to \bar{t}t$)	2·5
$W+(H \to \bar{t}t)_{120GeV}$	O(10)	$(\bar{q}q \to W)$(gg or $\bar{q}q \to \bar{t}t$)	1·5
$gg \to (H \to WW)_{200GeV}$	O(10)	$(\bar{q}q \to W)(\bar{q}q \to W)$	0·9
$WW \to (H \to WW)_{400GeV}$	1	$(\bar{q}q \to W)(\bar{q}q \to W)$	0·9
$\bar{t}t+(H \to WW)_{200GeV}$	1	$(\bar{q}q \to WW)$(gg or $\bar{q}q \to \bar{t}t$)	$1{\cdot}5 \times 10^{-3}$
$W+(H \to WW)_{200GeV}$	3	$(\bar{q}q \to WW)(\bar{q}q \to W)$	9×10^{-4}
$W+(H \to WW)_{200GeV}$	3	$(\bar{q}q \to W)(\bar{q}q \to W)(\bar{q}q \to W)$	3×10^{-6}

If $2m_W < m_H < 400$ GeV the dominant decays of the Higgs are into W^+W^- or Z^oZ^o. Now the dominant physics backgrounds come from $q\bar{q} \to W^+W^-$ or Z^oZ^o, and from the double process $(\bar{q}q \to W^+$ or $Z^o)(\bar{q}q \to W^-$ or $Z^o)$. The total cross-section[62] for $\bar{q}q \to W^+W^-$ and Z^oZ^o are shown in fig. 27 as functions of $\sqrt{s}$. We see from the Table that these are much larger than the double-subprocess cross-section estimated using the Ansatz (3.9), and therefore we have concentrated on the $\bar{q}q \to W^+W^-$ background to an H search. The encouraging

feature of this background is that it falls very rapidly with increasing $m(W^+W^-)$, as seen in fig.28: this means that the background is smaller for heavier Higgses $m_H >> 2m_W$. Another encouraging feature is that the intermediate boson pairs have final state angular distributions [62] which are sharply peaked forward and backward, as seen in fig.29. In contrast, Higgses decay isotropically in their centre-of-mass, which yields a Jacobian peak in the p_T of the final state $W^\pm$ or Z°. The ratios between the $\bar{q}q \to W^+W^-$ or $Z^\circ Z^\circ$ cross-sections of fig.27 and the $gg \to H$ cross-section shown in fig.13 are so large that we do not expect $gg \to H$ to be observable, except possibly if one optimizes cuts on the final state W and Z° distributions. It is possible to enhence the signal to background ratios by a factor 3(5)(7)(8) for m_H = 4(6)(8)(10) m_W by selecting events where WW pair emerge within 90° ± 30° in their centre-of-mass. We are more optimistic if one looks for the reactions gg or $\bar{q}q \to H\bar{t}t$ or $\bar{q}q \to V+H$. In both cases the double-subprocess backgrounds from $(\bar{q}q \to VV)(gg \text{ or } \bar{q}q \to \bar{t}t)$ or $(\bar{q}q \to V)(\bar{q}q \to VV)$ are smaller than the signal, as seen in Table 3. While the total rates for $H\bar{t}t$ or V+H production are quite small, they may offer the best modes for H detection in this mass range.

If $m_H > 400$ GeV the dominant Higgs cross-section is $WW \to H$ and the dominant background is $(\bar{q}q \to VV)$. The $(\bar{q}q \to V)(\bar{q}q \to V)$ background is concentrated at small $p_T << m_W$, and so cannot be confused with massive H decay which produces vector bosons V with $p_T >> m_W$. Simply looking at the VV invariant mass distribution will not be enough, because such a heavy Higgs is a wide resonance (fig.4). However, the angular distributions of the vector boson pairs in their centre-of-mass are completely different: isotropic in the s-wave H VV decay but sharply peaked in $\bar{q}q \to VV$. Therefore it may be possible to detect such a heavy Higgs by looking for deviations from the peaked angular distributions shown in fig.29.

Since in looking for $m_H > 200$ GeV we have to battle with low rates, it will be important to be able to detect a large fraction of H decays. This means being able to detect a large fraction of $W^\pm$ and Z° decays. In particular, when looking at W^+W^- and $Z^\circ Z^\circ$ pairs, one should be able to detect at least one vector boson by its hadronic decays. The rates will be too low if one can only use leptonic $W \to l\nu$ or $Z^\circ \to l^+l^-$ decays and the final states may be insufficiently constrained, if one must contend with the two missing neutrinos from $2W \to l\nu$ decays. It is clear that there will be large backgrounds to the hadronic decay modes from QCD jet production [10]. We have not evaluated them because they are very detector-dependent, and we have prefered to concentrate on backgrounds due to readily quantifiable physics processes. It may be that one can obtain better jet energy resolution and hence dijet mass resolution for heavier Higgses which decay into W's and hence jets with larger p_T: also the QCD background will be smaller at larger p_T. Our preliminary analysis already makes it clear that looking for Higgses at a high-energy hadron-hadron collider will not be easy. However, there may be hope for detecting Higgses by looking for V+H final states if $m_H < 400$ GeV, (H VV) + $\bar{t}t$ if 200 GeV < m_H < 400 GeV, and wide angle $(H \to VV)$ final states if $m_H > 400$ GeV.

3.3 - Supersymmetric Particles

We concentrate on the production of strongly interacting supersymmetric particles, namely squarks $\tilde{q}$ and gluinos $\tilde{g}$, since they have the largest cross-sections (3.5) for a given mass, and seem likely to make the largest possible mass range accessible for any given cross-section sensitivity.

3.3.1 - gluino pairs

The dominant perturbative QCD mechanism for $\tilde{g}\tilde{g}$ production is likely to be gg fusion, followed by $\bar{q}q$ annihilation. The subproces cross-section for $gg \to \tilde{g}\tilde{g}$ is[39]

$$\frac{d\hat{\sigma}}{d\hat{t}}(gg \to \tilde{g}\tilde{g}) = \frac{9\pi\alpha_s^2}{4\hat{s}^2}\left\{\frac{2(m_{\tilde{g}}^2-\hat{t})(m_{\tilde{g}}^2-\hat{u})}{\hat{s}^2} + \left[\frac{(m_{\tilde{g}}^2-\hat{t})(m_{\tilde{g}}^2-\hat{u})-2m_{\tilde{g}}^2(m_{\tilde{g}}^2+\hat{t})}{(m_{\tilde{g}}^2-\hat{t})^2} + (\hat{t}\leftrightarrow\hat{u})\right]\right.$$
$$\left. + \frac{m_{\tilde{g}}^2(\hat{s}-4m_{\tilde{g}}^2)}{(m_{\tilde{g}}^2-\hat{t})(m_{\tilde{g}}^2-\hat{u})} - \left[\frac{(m_{\tilde{g}}^2-\hat{t})(m_{\tilde{g}}^2-\hat{u})+m_{\tilde{g}}^2(\hat{u}-\hat{t})}{\hat{s}(m_{\tilde{g}}^2-\hat{t})} + (\hat{t}\leftrightarrow\hat{u})\right]\right\} \quad (3.19)$$

while that for $\bar{q}q \to \tilde{g}\tilde{g}$ is [39]

$$\frac{d\hat{\sigma}}{d\hat{t}}(q\bar{q}\to\tilde{g}\tilde{g}) = \frac{8\pi\alpha_s^2}{9\hat{s}^2}\left\{\frac{4}{3}\left(\frac{m_{\tilde{g}}^2-\hat{t}}{m_q^2-\hat{t}}\right)^2 + \frac{4}{3}\left(\frac{m_{\tilde{g}}^2-\hat{u}}{m_q^2-\hat{t}}\right)^2 + \frac{3}{\hat{s}^2}\left[(m_{\tilde{g}}^2-\hat{t})^2+(m_{\tilde{g}}^2-\hat{u})^2+2m_{\tilde{g}}^2\hat{s}\right]\right.$$
$$\left. \frac{\left[(m_{\tilde{g}}^2-\hat{t})+m_{\tilde{g}}^2\hat{s}\right]}{\hat{s}(m_{\tilde{q}}^2-\hat{t})} - \frac{3\left[(m_{\tilde{g}}^2-\hat{u})^2+m_{\tilde{g}}^2\hat{s}\right]}{\hat{s}(m_{\tilde{q}}^2-\hat{u})} + \frac{1}{3}\frac{m_{\tilde{g}}^2\hat{s}}{(m_{\tilde{q}}^2-\hat{t})(m_{\tilde{q}}^2-\hat{u})}\right\} \quad (3.20)$$

The total cross-section for $\tilde{g}\tilde{g}$ production is only weakly sensitive to $m_{\tilde{q}}$, as long as $m_{\tilde{q}} \gtrsim m_{\tilde{g}}$ (see fig.30) and $m_{\tilde{g}} < 1$ TeV. In what follows we generally present cross-sections calculated with $m_{\tilde{q}} = m_{\tilde{g}}$. We see immediately from fig.24 that the total cross-section for $\tilde{g}\tilde{g}$ production is larger than 1/10 pb for

$$m_{\tilde{g}} \begin{cases} \lesssim 1 \text{ TeV} & \sqrt{s} = 10 \text{ TeV} \\ \lesssim 1.6 \text{ TeV} & \sqrt{s} = 20 \text{ TeV} \\ \lesssim 2.4 \text{ TeV} & \sqrt{s} = 40 \text{ TeV} \end{cases} \quad (3.21)$$

This confirms our general observation (3.6) that the accessible range of new particle masses increases roughly as $\sqrt{s}^{\frac{1}{4}}$. The results (3.21) mean that any collider with $\sqrt{s} \lesssim 10$TeV can probe all the expected (2.13) range of gluino masses: the next step is to figure out the signatures for $\tilde{g}\tilde{g}$ production.

As we mentioned in section 2, we expect $\tilde{g} \to q\bar{q}\tilde{\gamma}$ decays to dominate. Another possibility is $\tilde{g} \to g\tilde{\gamma}$ via quark and squark loops [63], but this is expected to be a relatively unimportant decay mode:

$$\frac{\Gamma(\tilde{g}\to g+\tilde{\gamma})}{\Gamma(g\to q\bar{q}\tilde{\gamma})} \simeq \frac{3\alpha_s}{4\pi}\frac{(m_{\tilde{q}_R}^2 - m_{\tilde{q}_L}^2)^2}{(m_{\tilde{q}_L}^4+m_{\tilde{q}_R}^4)} \ll 1 \quad (3.22)$$

The presence in the final state of two photinos $\tilde{\gamma}$, which are expected in many models [37] to have masses much less thant $m_{\tilde{g}}$, typically

$$\frac{m_{\tilde{\gamma}}}{m_{\tilde{g}}} = \frac{8\alpha}{3\sin^2\theta_W \alpha_s} \tag{3.23}$$

means that one expects a large missing transverse energy-momentum signature:

$$p_T^{miss} = O(0.4 m_{\tilde{g}}) \tag{3.24}$$

Fig. 31 shows the missing p_T for different values of $m_{\tilde{g}}$. We see that the expectation (3.24) is borne out. A typical calorimetric experiment such as UA1 has a resolution [64] in p_T which is proportional to $E_T^{\frac{1}{2}}$:

$$\sigma \equiv \Delta p_T = 0.7 \sqrt{E_T} \tag{3.25}$$

Present collider extend up to E_T = O(200) GeV, and events are selected [4] as having a "interesting" missing p_T signature if $p_T^{miss} > 4\sigma$. We apply a similar cut to our sparticle production cross-sections, where E_T is computed from the "visible" q and $\bar{q}$ jet decay products.

We see from fig.32 that the total $\tilde{g}\tilde{g}$ cross-section is not greatly reduced by such a cut if $m_{\tilde{g}} \gtrsim$ O(100) GeV. We in any case expect the gluino to have been discovered before the start-up of a Large Hadron Collider if $m_{\tilde{g}} \lesssim$ O(100) GeV. The $p_T^{miss} > 4\sigma$ cut has a negligible effect on the total $\tilde{g}\tilde{g}$ cross-section for large $m_{\tilde{g}}$ = O(1) TeV, close to the limit of cross-section sensitivity.

We have computed the final state distributions for the final state jets coming from $\tilde{g} \to q\bar{q}\tilde{\gamma}$ decay. Their rapidity distribution is shown in fig.33: it is central with $\langle y^2 \rangle^{\frac{1}{2}} = 1.1$, in accord with our general expectations (fig.10). Even the smallest of the 4 jets coming from $\tilde{g}\tilde{g}$ production has sizeable p_T: fig.34 shows the distribution in p_T of the minimum p_T jet. We find

$$\langle p_T^{\text{min jet}} \rangle \approx 140 \text{ GeV} \quad \text{for } m_{\tilde{g}} = 1 \text{ TeV} \tag{3.26}$$

Since most of the gluino pairs are produced quite centrally, and decay quite isotropically, we expect large angular separations $\Delta\alpha$ between the different q and $\bar{q}$ jets. Indeed we find

$$\langle \Delta\alpha \rangle \approx 1.6 \text{ radians for } m_{\tilde{g}} = 1 \text{ TeV} \tag{3.27}$$

Since the angular resolution for jets at these energies is expected to be a few degrees, there should be no difficulty in distinguishing the 4 final state jets.

Thus $\tilde{g}\tilde{g}$ final states should be quite distinctive: 4 widely separated final state jets, each with $\langle p_T \rangle \gtrsim$ O(100) GeV, and large p_T^{miss}.

3.3.2 - Squark pairs

The dominant mechanism for $\tilde{q}\bar{\tilde{q}}$ pair production are again gg fusion and $\bar{q}q$ annihilation. The total subprocess cross-section for $gg \to \tilde{q}\bar{\tilde{q}}$ is [39]

$$\hat{\sigma}(gg\to\tilde{q}\,\bar{\tilde{q}}) = \frac{N_{\tilde{q}}\pi\alpha_s^2}{3\hat{s}}\left[\left(\frac{31}{64}+\frac{133}{16}\frac{m_{\tilde{q}}^2}{\hat{s}}\right)\xi + \left(4+\frac{m_{\tilde{q}}^2}{\hat{s}}\right)\frac{m_{\tilde{q}}^2}{\hat{s}}\ln\left(\frac{1-\xi}{1+\xi}\right)\right] \tag{3.28}$$

where

$\xi \equiv \sqrt{1-4m_{\tilde{q}}^2/s}$, and $N_{\tilde{q}}$ is the number of squark flavours available,

while the differential cross-section that for $\bar{q}q \to \tilde{q}\bar{\tilde{q}}$ is [39]

$$\frac{d\hat{\sigma}}{d\hat{t}}(q\bar{q}\to\tilde{q}\bar{\tilde{q}}) = \frac{2\pi\alpha_s^2}{9\hat{s}}\left\{\frac{2}{(m_{\tilde{g}}^2-\hat{t})^2}\left[\hat{s}(m_{\tilde{g}}^2-\hat{t})-(m_{\tilde{q}}^2-\hat{t})\right.\right.$$
$$-\frac{2}{3}\frac{1}{\hat{s}(m_{\tilde{g}}^2-\hat{t})}\left[(m_{\tilde{q}}^2-\hat{t})(\hat{u}-\hat{t})+\hat{s}(m_{\tilde{q}}^2+\hat{t})\right] \tag{3.29}$$
$$\left.\left.+\frac{N_{\tilde{q}}}{\hat{s}}\left[\hat{s}(\hat{s}-4m_{\tilde{q}}^2)-(\hat{u}-\hat{t})^2\right]\right\}$$

if the q and $\bar{q}$ have the same flavours, and [39]

$$\frac{d\hat{\sigma}}{d\hat{t}}(q\bar{q}'\to\tilde{q}\bar{\tilde{q}}') = \frac{4\pi\alpha_s^2}{9\hat{s}^2}\left\{\frac{1}{(m_{\tilde{g}}^2-\hat{t})}\left[\hat{s}(m_{\tilde{g}}^2-\hat{t})-(m_{\tilde{q}}^2-\hat{t})^2\right]\right\} \tag{3.30}$$

if they have different flavours. In most models the different flavours of $\tilde{q}$ have almost the same mass. Therefore, in what follows we have added together all the cross-sections for different flavours of $\tilde{q}\bar{\tilde{q}}$ production. We see from fig.35 that the total cross-section for $\tilde{q}\bar{\tilde{q}}$ production is quite sensitive to the gluino mass. If we assume conservatively that $m_{\tilde{g}} >> m_{\tilde{q}}$, then we see from fig.35 that the total cross-section for $\tilde{q}\bar{\tilde{q}}$ production is larger 1/10 pb for

$$m_{\tilde{q}} \lesssim \begin{cases} 900\ \text{GeV} & \sqrt{s} = 10\ \text{TeV} \\ 1.4\ \text{TeV} & \sqrt{s} = 20\ \text{TeV} \\ 2\ \text{TeV} & \sqrt{s} = 40\ \text{TeV} \end{cases} \tag{3.31}$$

in accord with the rule of thumb (3.6). Again we see from the results (3.31) that any collider with $\sqrt{s} \gtrsim 10$ TeV can explore essentially all the expected (2.13) range of squark masses.

If $m_{\tilde{g}} < m_{\tilde{q}}$, we expect the dominant decay mode of the $\tilde{q}$ to be $q + \tilde{g}$:

$$\frac{\Gamma(\tilde{q}\to q+\tilde{g})}{\Gamma(q\to q+\gamma)} = \frac{4}{3}\frac{\alpha_s}{\alpha}\left(\frac{1}{e_q}\right)^2 \tag{3.32}$$

In this case we would expect the $\tilde{g}$ to decay subsequently into $q\bar{q}\tilde{\gamma}$, and the p_T^{miss} signature to be somewhat diluted by comparison with that (3.24) for gluinos:

$$\langle p_T^{miss}\rangle = O(0.3m_{\tilde{q}}) \tag{3.33}$$

Fig.36a shows the missing p_T distribution for different combinations of $\tilde{q}$ and $\tilde{g}$ masses. We see that the expectation (3.33) is indeed borne out, and that the $p_T^{miss} > 4\sigma$ cut mentioned earlier has a negligible effect on the interesting cross-section for large $m_{\tilde{q}}$ (fig.37a). The final state missing p_T signature would be even more dramatic if $m_{\tilde{g}} > m_{\tilde{q}}$, so that $\tilde{q} \to q + \tilde{\gamma}$ decays dominate (fig.36b, 37b). In this case we would expect

$$\langle p_T^{miss} \rangle = O(\tfrac{1}{2} m_{\tilde{q}}) \tag{3.34}$$

as seen in fig.36b.

In the case of $\tilde{q} \to q + \tilde{g}$, $\tilde{g} \to q + q + \tilde{\gamma}$ decay we would expect 6 final state jets. The rapidity distribution for these jets in the case $m_{\tilde{q}} = 1$ TeV, $m_{\tilde{g}} = 700$ GeV is shown in fig.38. We find that

$$\langle y^2 \rangle^{\frac{1}{2}} = 1.2 \tag{3.35}$$

in accord with the expectation of fig.10. The p_T of each jet is of course somewhat smaller than was the case in direct $\tilde{g}\tilde{g}$ production. Fig.39 shows the p_T distribution for the minimum p_T jet, which has

$$\langle p_T^{\text{min jet}} \rangle \approx 90 \text{ GeV} \tag{3.36}$$

in the case $m_{\tilde{q}} = 1$ TeV, $m_{\tilde{g}} = 700$ GeV. This should nevertheless be large enough to be detectable. As expected, the angular separation $\Delta\alpha$ between the pairs of jets in $\tilde{q} \to q + \tilde{g}$, $\tilde{g} \to q + \bar{q} + \tilde{\gamma}$ decay is somewhat smaller

$$\Delta\alpha = 1.4 \text{ radians for } \begin{matrix} m_{\tilde{q}} = 1 \text{ TeV} \\ m_{\tilde{g}} = 700 \text{ GeV} \end{matrix} \tag{3.37}$$

than was the case (3.27) for direct $\tilde{g}$ production and decay. The angular separation (3.37) is nevertheless large enough for all 6 final state jets to be separated, providing a distinctive event signature. In the cas $m_{\tilde{g}} > m_{\tilde{q}}$ so that $\tilde{q} \to q + \tilde{\gamma}$ decay dominates, we expect the final state missing p_T to be larger than in $\tilde{q} \to q + \tilde{g}$ (see fig.36b). There will be 2 jet final states, for $m_{\tilde{q}} = 1$ TeV. The average p_T and angular separations of these two jets will surely be sufficient for them to be detected and separated easily.

Thus we expect $\tilde{q}\bar{\tilde{q}}$ production to produce distinctive 6 or 2-jet final states with large missing p_T. In addition, we note that a large fraction of the $\tilde{q}$ produced will have heavy flavours ($\tilde{c}$, $\tilde{b}$ or $\tilde{t}$), providing an additional final state event signature: $\tilde{c}$ or $\tilde{b}$ or $\tilde{t} \to$ (c or b or t) + ($\tilde{g}$ or $\tilde{\gamma}$).

3.3.3 - Sparticles in the proton

In addition to the perturbative QCD sparticle production by gg or $\bar{q}q$ collisions that we have discussed so far, there are other possible sources of sparticles in hadron-hadron collisions. In particular, it is possible that protons may already appear to contain sparticles when they are observed on a sufficiently high momentum scale. As was already discussed in connection with heavy quarks, this component may either be generated perturbatively (flavour excitation) or may be present nonperturbatively (intrinsic). Calculations have been made [65] of the perturbative generation of a sparticle content in the proton. They indicate that at infinite Q^2 the momentum of the proton is shaved out in the following way between quarks, gluons, squarks and gluinos:

Table 4: Asymptotic perturbative sparticle momentum fractions in the proton

	Pure QCD	QCD + $\tilde{g}$	QCD + $\tilde{q}$	QCD + $\tilde{g}$ + $\tilde{q}$
$q + \bar{q}$	$\frac{3N_q}{16+3N_q}$ (0.53)	$\frac{3N_q}{20+3N_q}$ (0.47)	$\frac{3N_q}{16+5N_q}$ (0.39)	$\frac{3N_q}{20+5N_q}$ (0.36)
g	$\frac{16}{16+3N_q}$ (0.47)	$\frac{16}{20+3N_q}$ (0.42)	$\frac{16}{16+5N_q}$ (0.35)	$\frac{16}{20+5N_q}$ (0.32)
g	—	$\frac{4}{20+3N_q}$ (0.11)	—	$\frac{4}{20+5N_q}$ (0.08)
$\tilde{q} + \bar{\tilde{q}}$	—	—	$\frac{2N_q}{16+5N_q}$ (0.26)	$\frac{2N_q}{20+5N_q}$ (0.24)

the total number of quark flavours is denoted by N_q, the figures in parentheses are the fractions obtained if $N_q = 6$. The perturbative QCD sparticles start from 0 at $Q^2 \lesssim m^2_{\tilde{q}}, m^2_{\tilde{g}}$, and are always smaller at finite Q^2 than the values in Table 4. Since cross-sections [66] with initial state sparticles (e.g. $\tilde{g} + g \to \tilde{g} + g$) are of the same order of magnitude as sparticle production cross-sections in collisions of normal partons (e.g. $g+g \to \tilde{g}+\tilde{g}$), we do not expect the production of heavy final state sparticles from initial perturbative sparticles in the proton to exceed the cross-sections we have presented in previous subsections. Indeed, since the initial sparticle distributions are small (i.e. $O(\alpha_s)$) at $Q^2 = O(m^2_{\tilde{q}}, m^2_{\tilde{g}})$, we expect the dominant contributions to heavy sparticle production to come from normal parton collisions: gg or $q\bar{q} \to \tilde{g}\tilde{g}$ or $\tilde{q}\bar{\tilde{q}}$. However, ($\tilde{g}$ or $\tilde{q}$) + (g or q) $\to$ ($\tilde{g}$ or $\tilde{q}$) + (g or q) subprocesses have interesting event signatures: one sparticle at large P_T and the other in one of the beam fragmentation regions. This type of reaction may, however, be interesting if $m_{\tilde{q}}$ or $m_{\tilde{g}}$ is just above the limit from present-day accelerators say $m_{\tilde{q}}$ or $m_{\tilde{g}} \lesssim 100$ GeV.

It is possible that there may be a large nonperturbative intrinsic sparticle component in the proton, just as has been postulated [52] for charm and heavier quarks. This picture may be either confirmed or refuted by searches [67] for diffractive t quark

production at the CERN $p\bar{p}$ Collider. In the absence of any better experimental guide, we assume the form of diffractive cross-section postulated [52] by theorists:

$$\sigma(?, \sqrt{s}) = \frac{1}{m_?^2} f\,(m_?/\sqrt{s}) \tag{3.38}$$

We assume a universal scaling function f for heavy quarks, squarks and gluinos. Then we can scale up from m_c = 1.5 GeV, $\sqrt{s}$(ISR) = 60 GeV, σ (m_c, 60 GeV) $\approx$ 100 pb to deduce

$$\sigma\,(m_{\tilde{q}} \text{ or } m_{\tilde{g}} = \tfrac{1}{2}\ \text{TeV},\ \sqrt{s} = 20\ \text{TeV}) \approx\ O(1)\text{nb} \tag{3.39}$$

Even if this is a grotesque overestimate - perhaps cross-sections scale as $m_?^{(-n \geq 3)}$ instead of n = 2 in equation (3.38)? - it suggests that there may be observable diffractive cross-sections for the production of sparticle pairs weighing up to O(1) TeV.

The signature for such events would be two sparticles moving forward in one hemisphere, while the other hemisphere is quiet. It has been proposed [68] that one may estimate the t quark mass from diffractively produced $T \equiv (t\bar{q})$ meson decays into $b\bar{q}+\mu^+ + \nu$ final states by computing the minimum transverse mass (or cluster transverse mass)

$$m^* \equiv [\, m_{vis}^2 + 2p_T^{miss\,2} + 2p_T^{miss}\,(m_{vis}^2 + p_T^{miss\,2})^{\frac{1}{2}}\,]^{\frac{1}{2}} \tag{3.40}$$

which is theoretically expected to be sharply peaked at $\xi \equiv m^*/m_t \approx 1$. In the case of heavy quarks, one might expect the meson to have a smaller mean $x_F \equiv E/E_{beam}$, and thereby avoid any misidentification of meson and baryon decay products. The same might also be true for $\tilde{q}$ hadrons: perhaps $x_F(\tilde{q}qq) > x_F(\bar{\tilde{q}}q)$? but it might be that both gluino hadrons would have similar values of x_F. In this case, if one seeks to estimate $m_{\tilde{g}}$ by looking for a peak in $\xi \equiv m^*/m_{\tilde{g}}$, where m* is computed from a pair of observed jets deemed to come from $\tilde{g} \to q\bar{q}\tilde{\gamma}$ decay, one must contend with a combinatorial background due to the misidentification of which jets come from the decay of which gluino hadron. However, as seen in fig.40, this may not be an overwhelming background [69], and one should still be able to see a nice peak in m* and thereby estimate $m_{\tilde{g}}$ in diffractive events. Looking for evidence of diffractive squark production would be even easier if $\tilde{q} \to q + \tilde{\gamma}$ decays dominate. In this case there would be a Jacobian peak in the observed jet p_T in diffractive events with large missing p_T.

3.3.4 - Observability

It is difficult to think of large physics backgrounds to the missing p_T signature of susy. Present-day collider data [3,4] are already encouraging, in that it has been possible to extract a sample of events with significant missing p_T which have a cross-section no larger that that for $\bar{p}p \to W + x$, $W \to l\nu$, and are not overwhelmed by backgrounds due to physics or instrumental effects. As mentioned earlier, we do not discuss instrumental backgrounds (jet and calorimeter fluctuations, holes in the apparatus, etc.) as they depend strongly on the detector characteristics assumed [40]. The dominant physics background is likely to be from heavy flavour pair production and semileptonic decay:

c or b or $t \to \nu + l^{\pm} + q$, where the final state charged lepton is not detected and the neutrino carries away a large amount of p_T. While $e^{\pm}$ can only be detected if they have relatively large p_T ($\gtrsim$ O(50) GeV?), it should be possible to detect $\mu^{\pm}$ with p_T above a few GeV. Thus a large part of the heavy flavour background ($\nu_\mu + \mu^{\pm} + q$) can be measured, and the rest ($\nu_e + e^{\pm} + q$, $\nu_\tau + \tau^{+} + q$) will have a similar magnitude. Most of the background events will have 2 jets, and the missing p_T vector will be aligned essentially parallel to one of the jet axes in the azimuthal angle plane. There will be some fraction of multiple jets due to gluon bremsstrahlung and other higher order QCD effects, but the missing p_T vector will always be essentially parallel to one of the jets. We have not studied the heavy flavour background itself, but have looked at the distribution in p_T^{miss} transverse to the observed jets in $\tilde{g}$ decay. We see in fig.41 that the distribution in missing p_T transverse to the nearest jet axis is relatively wide, certainly much wider than the $O(\frac{m_{c \text{ or } b \text{ or } t}}{2})$ which one would expect from heavy flavour production. We therefore expect that the heavy flavour background can be dealt with, as it seems to be at the present Collider [4]. This expectation is supported by the analysis of an experimental working group [40] at this Workshop.

We conclude that detecting supersymmetric particles weighing less than the expected upper limit of order 1 TeV should be relatively easy at any hadron-hadron collider with $\sqrt{s} \lesssim$ 10 TeV.

3.3.5 - Alternative supersymmetry phenomenologies

So far we have explored the conventional phenomenological supersymmetry scenario, in which the lightest sparticle is the photino $\tilde{\gamma}$, and R-parity is conserved so that every sparticle must have a $\tilde{\gamma}$ among its decay products, e.g. $\tilde{q} \to q + \tilde{\gamma}$, $\tilde{g} \to q + \bar{q} + \tilde{\gamma}$. In this subsection we explore two alternative phenomenological scenarios : either (I) the gluino is (almost) the lightest sparticle, R-parity is conserved as usual, and the gluino is (almost) stable[70], or (II) R-parity is broken[38,71,72,73].

(I) In the context of a collider experiment, a new particle appears stable if it strikes the calorimeter before decaying. This requires $\gamma c\tau > O(1)$ metre, or

$$\tau > 10^{-9}\ (10^{-10})\ \text{sec} \quad \text{if } \gamma = 3(30) \tag{3.41}$$

For this to occur, the momentum release in $\tilde{g}$ decay should probably be less than a GeV. This could well be the case if $m_{\tilde{g}}$ is a few GeV, but seems unlikely if $m_{\tilde{g}} > O(10)$ GeV, and is excluded if the $\tilde{\gamma}$ and $\tilde{g}$ masses are in the canonical ratio (3.23) which is smaller than about 1/7. It could well be that the canonical ratio (3.23) is incorrect, but even if it is, we find it unreasonable that $m_{\tilde{g}} - m_{\tilde{\gamma}} < 1$ GeV if $m_{\tilde{g}} > O(10)$ GeV, though this could be a possibility if $m_{\tilde{g}} < O(10)$ GeV. When $m_{\tilde{g}} > O(10)$ GeV, we believe that the only reasonable alternative to the conventional assumption is to postulate that the canonical ratio (3.23) is so wrong that the gluino is actually the lightest sparticle. We therefore retain as logical possibilities $m_{\tilde{g}} < O(10)$ GeV and either absolutely or almost stable, or $m_{\tilde{g}} > O(10)$ GeV and absolutely stable.

If the gluino is absolutely stable, the lightest gluino hadron should be neutral, otherwise there will be a conflict with upper limits[29] on stable charged hadrons coming from e^+e^- annihilation ($m_{\pm} < O(20)$ GeV) or from searches[79] for exotic isotopes containing relic gluino hadrons left over from the Big Bang ($m_{\pm} < O(1)$ TeV). Searches for exotic isotopes and mass spectrometer experiments also exclude stable neutral gluino hadrons if they weigh more than about 3 GeV. Therefore stable gluinos should weigh less than about 3 GeV. The existence of such objects seems not to conflict with any present-day particle physics experiment[70,75]. The best place to look today for such stable gluinos may be[65] in the decay of P-wave states of bottomonium P_b. These are expected[65] to have a branching ratio of order 30% into pairs of such light gluinos. A systematic search of P_b decays could surely reveal whether such a large fraction of final states contained a pair of stable or almost stable gluino hadrons.

We do not think that a very high energy hadron collider, or even the present CERN $p\bar{p}$ Collider, is the ideal place to look for light stable or almost stable gluinos ($m_{\tilde{g}} < O(10)$ GeV). It may nevertheless be interesting to point out a possible signature, namely the production of a pair of large p_T jets which each contain an energetic neutral particle that is undetectable in the central tracking detector, but deposits its energy in the hadronic (not electromagnetic) calorimeter, causing a mismatch between the energy-momentum measurements in the central detector and in the calorimeters. Of course, such events occur all the time, thanks to neutron and K_L^0 production. However, when one of these particles is produced in one jet, there is no reason to expect another one in the

opposite large p_T jet, though this should occur inevitably in $\tilde{g}\tilde{g}$ production events. Moreover, if $m_{\tilde{g}} \gtrsim O(m_c) \approx 1.5$ GeV, one could expect the neutral gluino hadron to carry on average a half of each large p_T jet energy, whereas neutrons and K_L^0's are generally softer. A search for such anomalous calorimetry events at lower centre-of-mass energies might be valuable.

(II) Two possible mechanisms for R-parity violation have been considered in the literature - explicit breaking through soft supersymmetry breaking or superpotential terms[71], and spontaneous breaking through sneutrino vacuum expectation values[72]. For reasons of elegance and simplicity we restrict ourselves to spontaneous R-parity breaking, which may come about through $v_e \equiv \langle 0|\ \tilde{\nu}_e|0\rangle \neq 0$, $v_\mu \equiv \langle 0|\tilde{\nu}_\mu|0\rangle \neq 0$ or $v_\tau \equiv \langle 0|\ \tilde{\nu}_\tau|0\rangle \neq 0$. Model studies[72] indicate that $v_\tau \neq 0$ whenever any other sneutrino develops a vacuum expectation value, and that in general $v_\tau > v_\mu > v_e$. Whenever a certain sneutrino acquires a vacuum expectation value, the corresponding lepton number L_ι is also spontaneously violated, but the modified parity $R_\iota \equiv R(-1)^{L_\iota}$ is conserved. The very stringent upper limits on violations of electron-number L_e and of muon-number L_μ impose small upper limits on v_e and v_μ. The upper limits on violation of tau-number L_τ are much less stringent, and v_τ could be quite large. In what follows we assume that only $v_\tau \neq 0$, while $v_e = v_\mu = 0$. In this case, although R-parity is violated, $R_\tau = R(-1)^{L_\tau}$ is conserved.

The consequences of R-parity breaking for the production and decays of sparticles are quite dramatic[76,73]. they need no longer be produced in pairs, they need not decay into other sparticles, and the lightest sparticle need not be stable. In general, sparticles can mix with particles having the same colour and electric charges. In the case considered here, R violation is always associated with L_τ violations, so sparticles may be produced in association with τ or ν_τ, sparticles may decay into τ or ν_τ, and colourless charged sparticles such as the $\tilde{W}^\pm$ and $\tilde{H}^\pm$ can mix with the $\tau^\pm$, while colourless neutral sparticles can mix with the ν_τ. Examples of posssible novel phenomena are in principle $Z^0 \to \tilde{\gamma} + \nu_\tau$, $\tilde{q} \to q + (\tau \text{ or } \nu_\tau)$ and $\tilde{\gamma} \to \tau^- e^+ \nu_e$ or $\nu_\tau e^+ e^-$ decays. In what follows we discuss briefly some qualitative features of such phenomena, the details being discussed elsewhere[73].

The $\tau^\pm$ mix with the $\tilde{W}^\pm$ and $\tilde{H}^\pm$ through a matrix of the form[72,73]

$$(\tilde{W}^+, \tilde{H}^+, \tau_o^+)_L \begin{pmatrix} M_2 & g_2 v & g_2 v_\tau \\ g_2 v' & \varepsilon & 0 \\ 0 & h_\tau v_\tau & m_{\tau_o} \end{pmatrix} \begin{pmatrix} \tilde{W}^- \\ \tilde{H}^- \\ \tau_o^- \end{pmatrix}_L \tag{3.42}$$

where M_2 is the SU(2) gaugino mass, ε is a term mixing the two Higgs multiplets H and H', v and v' are their vacuum expectation values, τ_o is the unmixed τ and m_{τ_o} is its mass before mixing with $\tilde{W}$ and $\tilde{H}$, and h_τ is the tau Yukawa coupling to the Higgs H. The physical tau mass eigenstate has mass

$$m_\tau = \frac{h_\tau (v^2 - v_\tau^2)}{\sqrt{v^2 + v_\tau^2}} \tag{3.43}$$

and the mixed components

$$\tau_L^+ = \tau_{0L}^+ - \frac{2h_\tau v v_\tau}{g_2(v^2+v_\tau^2)} \tilde{W}_L^+ \quad , \quad \tau_L^- = \frac{v\tau_{0L}^- - v_\tau \tilde{H}_2^-}{\sqrt{v^2+v_\tau^2}} \qquad (3.44)$$

We see from (3.44) that the physical τ_L^+ has only a small mixing with the $\tilde{W}_L^+$, because h_τ is small even though v_τ may not be much smaller than v, while the physical τ_L^- may have large mixing with the $\tilde{H}_L^-$ but not with the $\tilde{W}_L^-$. Since the H couplings to quarks and leptons are small, this unfortunately means that taus are unlikely[73] to be copiously produced in the decays of squarks and gluinos. An analogous study of the more complicated mixing matrix for the ν_τ^0, $\tilde{W}^0$, $\tilde{B}^0$, $\tilde{H}^0$ and $\tilde{H}'^0$ reveals that the physical ν_τ might have substantial mixing with the $\tilde{W}^0$ and $\tilde{B}^0$:

$$\nu_\tau = \nu_\tau^0 + O(\frac{\varepsilon}{m_W}) \frac{g_2\tilde{W}^0 + g_1\tilde{B}^0}{\sqrt{g_1^2+g_2^2}}$$

$$+ \tilde{H}^0, \tilde{H}'^0 \text{ components, higher orders in } \frac{\varepsilon}{m_W} \text{ , etc.} \qquad (3.45)$$

Therefore the ν_τ could in principle be copiously produced in $\tilde{q}$ and $\tilde{g}$ decays, but would give the same missing energy-momentum signature as that expected in conventional supersymmetric phenomenology. We find that mixing includes an off-diagonal neutral current coupling of the Z^0 to a H^0 and a ν_τ, which is proportional to $\frac{v_\tau}{\sqrt{v^2+v'^2}}$ and hence small if $v_\tau \ll v,v'$. Therefore in the model discussed here much of conventional supersymmetry phenomenology remains unchanged, except that the $\tilde{\gamma}$ can now decay. The lifetime of the $\tilde{\gamma}$ depends sensitively on its mass, but the mixing between the $\tilde{\gamma}$ and the ν_τ lifetime could well be long enough for its decay vertex to be separated from the interaction point.

Disappointingly, we have not discovered a strong likelihood for copious τ production in models with broken R-parity, though $\tilde{\gamma}$ decays may provide a signature for such models. This possibility should be borne in mind when planning searches for supersymmetric particles, though we still feel that the conventional sypersymmetric phenomenology discussed in previous sections is a more plausible scenario.

3.4 - Technicolour

As representative examples of technicolour particles, we have considered the production of coloured pseudoscalars P_8, octets V_8 and the techniquark continuum.

3.4.1 - Technipions P_8

These are expected to have masses O(250) GeV. The largest cross-section is[76,77] for neutral P_8^0 production via gg fusion :

$$\sigma\,(P_8^0) \;=\; \frac{\pi^2}{m^3_{P_8^\circ}}\;\; \Gamma\,(P_8^\circ \to gg)\;\tau L_{gg}(\tau) \tag{3.46}$$

where

$$\Gamma\,(P_8^\circ \to gg) \;=\; \frac{5}{3}\;\frac{G_F}{\sqrt{2}}\;\;\frac{M^3_{P_8^\circ}}{\pi}\;\left(\frac{\alpha_s}{\pi}\right)^2\;\left(\frac{N_{TC}}{4}\right)^2 \tag{3.47}$$

We take the number of technicolours $N_{TC} = 4$ as a representative example. The partial decay width (3.47) is much larger than that for decays into $\bar{q}q$ pairs, with the exception of $\bar{t}t$:

$$\Gamma\,(P_8^\circ \to \bar{t}t) \;=\; \frac{G_F}{\sqrt{2}}\;\;\frac{M_{P_8^\circ}}{\pi}\;\;m_t^2 \tag{3.48}$$

Comparing the total decay widths (3.37, 3.48), we see that the dominant decay mode of P_8° may be into $\bar{t}t$. The $P_8^\pm$ cannot be produced by gg fusion, but only by $u\bar{d}$ or $d\bar{u}$ fusion, which has a far smaller coupling than (3.48). Therefore we only compute the cross-section for P_8° production in hadron-hadron collisions, which is displayed in Fig. 42. The signature for P_8° production would be $P_8^\circ \to \bar{t}t$ decay.

3.4.2 - Technivectors V_8

Also shown in Fig. 42 are the cross-sections[76] for V_8° production :

$$\sigma\,(V_8^\circ) \;=\; \frac{3\pi^2}{m^2_{V_8^\circ}}\;\left[\;\Gamma\,(V_8^\circ \to gg)\;\tau L_{gg}(\tau) \;+\; \frac{32}{9}\;\Gamma\,(V_8^\circ \to \bar{u}u)\;\tau L_{u\bar{u}}(\tau)\right.$$

$$\left. +\; \frac{32}{9}\;\Gamma\,(V_8^\circ \to \bar{d}d)\;\tau L_{d\bar{d}}(\tau)\;\right] \tag{3.49}$$

where

$$\Gamma(V_8^\circ \to gg) \;=\; \frac{2\pi\alpha_s^2}{m_{V_8^\circ}}\;F_v^2 \quad : \quad F_v^2 \approx 2F_T^2 \;:\; F_T \approx 125\ \text{GeV} \tag{3.50a}$$

$$\Gamma(V_8^\circ \to u\bar{u} \;\text{ or }\; d\bar{d}) \;=\; \frac{4}{3}\;\frac{\pi\alpha_s^2}{m_{V_8^\circ}}\;\;F_v^2 \tag{3.50b}$$

We take $m_{V_8^\circ} = 900$ GeV. The gg fusion mechanism dominates over $u\bar{u}$ and $\bar{d}d$ annihilation by an order of magnitude. This means that $V_8^\pm$ production, which proceeds via $u\bar{d}$ or $\bar{u}d$ annihilation alone, is somewhat smaller than V_8° production, as seen also in fig. 42. We would expect the V_8° decay into $g + P_8^\circ$, by analogy with conventional QCD vector $\to$ pseudoscalar $+ \gamma$ decays, and also into $g + (\gamma \text{ or } Z^0)$, while the $V_8^\pm$ could decay into $W^\pm + g$.

3.4.3 - Technicolour Continuum

In addition to the production of particular technifermion-antifermion $Q_T\bar{Q}_T$ bound states, one can also estimate the total cross-section for continuum $Q_T\bar{Q}_T$ production by analogy with conventional heavy quark production. We assume the existence of 2 techniquarks U_T and D_T, each coming in $N_{TC} = 4$ technicolours, so that the production cross-section is 8 times larger than would naively be estimated by scaling up gg or $\bar{q}q \to \bar{t}t$.

The principal uncertainty of this estimate is the correct techniquark mass m_{Q_T} to be used. One expects it to be generated dynamically by the strong technicolour interactions, and to be somewhere in the range 300 GeV to 1 TeV. In fig. 42 we have plotted total cross-sections for $Q_T\bar{Q}_T$ continuum production for three possible values : 300 GeV, 500 GeV and 1 TeV. We guess that m_{Q_T} would lie in between the two lower values used : the highest value is a gesture to conservatism. In all cases the continuum production cross-section is likely to be large enough to be detectable at $E_{cm} \geq 10$ TeV, though the cross-section becomes rapidly more favourable for lower values of m_{Q_T} and larger values of E_{cm}. Presumably the final state resulting from $Q_T\bar{Q}_T$ continuum production would contain many technipions, including the P_8, other denizens of Table 2, and longitudinal components of the $W^{\pm}$ and Z^0. We have not attempted to estimate these, as they must be very model-dependent and our competence does not in any case extend to calculating strong technicolour dynamics.

3.4.4 - Observability

The main physics background to a search for $P_8^\circ \to \bar{t}t$ comes from QCD production of $\bar{t}t$ pairs via gg fusion or $\bar{q}q$ annihilation. At the centre-of-mass energies and $(\bar{t}t)$ invariant masses of interest to us, the dominant source of $(\bar{t}t)$ pairs is gg fusion. Since this is also the dominant source of P_8° production, the signal-to-background ratio is essentially independent[77] of E_{cm} and y in the range of interest to us. Assuming $m_{P_8^\circ} = 250$ GeV and $m_t = 35$ GeV we have calculated

$$\frac{\sigma\,(gg \to P_8^\circ \to \bar{t}t}{\sigma\,(gg \to \bar{t}t)} \approx \frac{1}{3} \quad : \quad \text{integrated over all } \theta^* \tag{3.51}$$

if one assumes 5% resolution in $m(\bar{t}t)$ and integrates over all the $(\bar{t}t)$ angular distribution. However, the rate for P_8° production is so large that one can afford to reduce it by making cuts in θ^*, the $(\bar{t}t)$ centre-of-mass angle relative to the beam axes. The $P_8^\circ \to \bar{t}t$ decays are of course isotropic in this variable, while $gg \to \bar{t}t$ is sharply peaked in the forward and backward directions, as seen in fig. 43. This means that one can improve the signal-to-background ratio by making cuts in θ^* :

$$\frac{\sigma\,(gg \to P_8^\circ \to \bar{t}t)}{\sigma\,(gg \to \bar{t}t)} = \begin{cases} 0.9 \text{ for } \left|\theta^* - \frac{\pi}{2}\right| < \frac{\pi}{4} \\ 1.5 \text{ for } \left|\theta^* - \frac{\pi}{2}\right| < \frac{\pi}{8} \end{cases} \tag{3.52}$$

where the overall reduction in signal rate is by a factor of 0.7 or 0.4 respectively. We conclude that it should be possible to detect the P_8°, if one can identify clearly $(\bar{t}t)$ jet pairs and get good invariant mass resolution around $m(\bar{t}t) \approx 250$ GeV. One is helped at a Large Hadron Collider by the large rate relative to those at the present CERN $\bar{p}p$ Collider and the forthcoming Tevatron Collider projects. We have not looked in detail at the physics backgrounds to a search for V_8° or $V_8^\pm$, which we fear may be substantial.

4. - Summary of important signatures

In this final section we catalogue some of the important signatures which experiments at large hadron colliders should be able to detect. We leave to our experimental colleagues the task of devising detectors which see them with high efficiency and low background. This will not be trivial in many cases, particulary those involving heavy particles which decay into hadronic jets. Any non-ideal detector would suffer from backgrounds additional to the "physics" backgrounds discussed in section 3.

$(\bar{t}t)$: useful for hunting Higgs bosons and technipions.

Multiple $W^{\pm}$, Z^{0} : Also useful for Higgs and technicolour searches. In view of the low rates for many Higgs production mechanisms, one should not rely solely on leptonic decay modes of the $W^{\pm}$ and Z^{0}, but should also have some efficiency for picking them out via their decays into hadronic jets. Experience from UA1 and UA2 indicates that this is not easy in events without an additional final state signature. It may be easier to pick out a second or third $W^{\pm}$ or $Z^{0} \rightarrow$ hadronic jet decay if the first $W^{\pm}$ or Z^{0} is already identified through a leptonic decay mode. Paying the price of a second or third leptonic decay branching ratio might leave an unobservable small rate.

Missing p_T : This is very important for supersymmetry searches, and a hermetic detector on the UA1 model seems to be essential. As already mentioned in section 3.3, searching for missing p_T is likely to be easier at higher energy colliders, since calorimeters have energy resolutions $\Delta E \propto \sqrt{E}$, whereas the missing p_T signal being sought probably increases roughly linearly with E.

jet-jet-mass bumps : Good dijet mass resolution is clearly important for the $\bar{t}t$, $W^{\pm}$ and Z^{0} searches previously mentioned, as well as for such signals as excited quark $\rightarrow q + g$ decay.

γ-jet mass bumps : Are also potentially useful in the search for excited quarks.

leptons, e, ν, τ, ... : It goes without saying that a high capability to detect these is a sine qua non for many of the other particle searches.

Based on the analyses of section 3, and on the likely cleanliness of the above signatures, we reach the following tentative conclusions about the difficulty of observing different species of new particles at a large hadron-hadron collider.

Supersymmetry : relatively easy

Technicolour : possible

Conventional Higgs boson : relatively difficult.

In general we are quite optimistic that a large hadron collider wuld make an important contribution to the exploration of physics in the mass range up to O(1) TeV where there is good reason to expect a rich harvest of new particles.

ACKNOWLEDGEMENTS

We would like to thank C. Jarlskog and Z. Kunszt for sharing with us their resutlts described in the paper.

References

1 - UA1 Collaboration, G. Arnison et al. - Phys. Lett. 122B, 103 (1983);
UA2 Collaboration, M. Banner et al. - Phys. Lett. 122B, 476 (1983).

2 - UA1 Collaboration, G. Arnison et al. - Phys. Lett. 126B, 398 (1983);
UA2 Collaboration, P. Bagnaia et al. - Phys. Lett. 129B, 130 (1983).

3 - UA2 Collaboration, P. Bagnaia et al. - Phys. Lett. 139B, 105 (1984)

4 - UA1 Collaboration, G. Arnison et al. - Phys. Lett. 139B, 115 (1984)

5 - UA2 Collaboration, J.D. Hansen - Talk presented at the 4th Workshop on $p\bar{p}$ Collider Physics, Bern (1984).

6 - UA1 Collaboration, C. Rubbia - Talk presented at the 4th Workshop on $p\bar{p}$ Collider Physics, Bern (1984).

7 - R. Barbieri - Talk presented at this meeting.

8 - R. Peccei - Talk presented at this meeting.

9 - C.H. Llewellyn Smith - Talk presented at this meeting.

10 - A. Ali - Talk presented at this meeting.

11 - B. Andersson - Talk presented at this meeting.

12 - G. Altarelli - Talk presented at this meeting.

13 - E.Eichten, I.Hinchliffe, K.D.Lane and C.Quigg - Fermilab-PUB-8417-T (1984).

14 - J.S. Bell - Nucl. Phys. B60, 427 (1973);
C.H. Llewellyn Smith - Phys. Lett. 46B, 233 (1973);
J. Cornwall, D.N. Levin and G. Tiktopoulos - Phys. Rev. Lett. 30, 1268 (1973) and Phys. Rev. D10, 1145 (1974).

15 - J. Ellis, M.K. Gaillard and D.V. Nanopoulos - Nucl. Phys. B106, 292 (1976).

16 - S.J. Freedman, J. Napolitano, J. Camp and M. Kroupa - Phys. Rev. Lett. 52, 240 (1984).

17 - S. Coleman and E. Weinberg - Phys. Rev. D7, 788 (1973);
S. Weinberg - Phys. Rev. Lett. 36, 294 (1976);
A.D. Linde - Pis'ma Zh. Eksp. Teor. Fiz. 23, 73 (1976);
E. Witten - Nucl. Phys. B177, 477 (1981).

18 - M. Veltman - Acta Phys. Pol. B8, 475 (1979);
C.E. Vayonakis - Lett. Nuov. Cim. 17, 383 (1976) and Athens Univ. preprint (1978).

19 - B.W. Lee, C. Quigg and H. Thacker - Phys. Rev. D16, 1519 (1977).

20 - S. Weinberg - Phys. Rev. D13, 974 (1976) and D19, 1277 (1979);
L. Susskind - Phys. Rev. D20, 2619 (1979).
For a review, see E. Farhi and L. Susskind - Phys. Rep. 74C, 277 (1981).

21 - Exotic particles Study Group, G. Barbiellini et al. - DESY preprint 79/27 (1979).

22 - B. Humpert - Phys. Lett. 131B, 461 (1983);
B. Humpert and R. Odorico - Talk at the 4th Workshop on $p\bar{p}$ Collider Physics, Bern(1984) and talk at this meeting.

23 - G. 't Hooft - "Recent Developments in Gauge Theories", ed. G. 't Hooft et al. (Plenum Press, N.Y., 1980).

24 - S. Hawking, D.N. Page and C.N. Pope - Phys. Lett. 86B, 175 (1979) and Nucl. Phys. B170 (FS1), 283 (1980).

25 - E. Gildener and S. Weinberg - Phys. Rev. D13, 3333 (1976);
E. Gildener - Phys. Rev. D14, 1667 (1976).

26 - A.J. Buras, J. Ellis, M.K. Gaillard and D.V. Nanopoulos - Nucl. Phys. B135, 66 (1978).

27 - S. Dimopoulos and L. Susskind - Nucl. Phys. B155, 237 (1979);
E. Eichten and K.D. Lane - Phys. Lett 90B, 125 (1980).

28 - S. Dimopoulos and J. Ellis - Nucl. Phys. B182, 505 (1981).

29 - S. Yamada - Proc. Int. Symposium on Lepton and Photon Interactions, Cornell 1983, ed. D.G. Cassel and D.L. Kreinick (Lab. of Nuclear Studies, Cornell, 1983), p. 529.

30 - For recent attempts, see M.A.B. Bég - Phys. Lett. 124B, 403 (1983);
S. Dimopoulos, H. Georgi and S. Raby - Phys. Lett. 127B, 101 (1983).

31 - Y. Gel'fand and E.P. Likhtman - Pis'ma Zh. Eksp. Teor. Fiz. 13, 323 (1971);
D. Volkov and V.P. Akulov - Phys. Lett. 46B, 109 (1973).
J. Wess and B. Zumino - Nucl. Phys. B70, 39 (1974).

32 - J. Wess and B. Zumino - Phys. Lett. 49B, 52 (1974);
J. Iliopoulos and B. Zumino - Nucl. Phys. B76, 310 (1974);
S. Ferrara, J. Iliopoulos and B. Zumino - Nucl. Phys. B77, 413 (1974).

33 - For a review, see P. Fayet and S. Ferrara - Phys. Rep. 32C, 249 (1977).

34 - CHARM Collaboration, F. Bergsma et al. - Phys. Lett 121B, 429 (1983);
E 613, R. Ball et al. - Univ. Michigan preprint UMHE 83/13/UWEX-83-234 (1983).

35 - J. Ellis and H. Kowalski - CERN preprint TH-3843 (1984) and DESY preprint 84-045 (1984).

36 - H. Goldberg - Phys. Rev. Lett. 50, 1419 (1983);
J. Ellis, J.S: Hagelin, D.V. Nanopoulos, K.A. Olive and M. Srednicki
Nucl. Phys. B238, 453 (1984)

37 - For a review, see J. Ellis - CERN preprint TH-3802 (1984).

38 - L.J. Hall and M. Suzuki - Nucl. Phys. B231, 419 (1984);
G.G. Ross and J. Valle - Oxford preprint in preparation (1984).

39 - G. Kane and J.P. Léveillé - Phys. Lett. 112B, 227 (1982);
P. Harrison and C.H. Llewellyn Smith - Nucl. Phys. B213, 223 (1982) and E B223, 542 (1983).

40 - For a discussion see P. Bagnaia and A. Weidberg - Contribution to this meeting.

41 - S. Dimopoulos - Nucl. Phys. B168, 69 (1980).

42 - S.D. Drell and T.-M. Yan - Phys. Rev. Lett. 25, 316 (1970).

43 - G. Altarelli and G. Parisi - Nucl. Phys. B126, 298 (1977).

44 - S. Berman, J.D. Bjorken and J. Kogut - Phys. Rev. D4, 3388 (1971).

45 - W. Furmanski and H. Kowalski - Nucl. Phys. B224, 523 (1983).

46 - CDHS Collaboration, H. Abramowicz et al. - Zeit. f. Phys. C13, 199 (1982) and F. Eisele - private communication (1984).

47 - E. Eichten et al. - ref. 13;
R. Baier, J. Engels and B. Petersson - Zeit. f. Phys. C2, 265 (1979);
M. Glück, E. Hoffman and E. Reya - Zeit. f. Phys. C13, 119 (1982).

48 - J. Ellis - SLAC preprint PUB-3127 (1983).

49 - I. Hinchliffe - Talk presented at the 4th Workshop on $p\bar{p}$ Collider Physics, Bern (1984), quoting results of ref. 13.

50 - J. Kuti and V.F. Weisskopf - Phys. Rev. D4, 3418 (1971).

51 - H. Georgi, S.L. Glashow, M. Machacek and D.V. Nanopoulos - Phys. Rev. Lett. 40, 692, (1978).

52 -S.J. Brodsky, C. Petersson and N. Sakai - Phys. Rev. D23, 2745 (1981);
V. Barger, F. Halzen and W.Y. Keung - Phys. Rev. D24, 1428 (1981);
R. Horgan and M. Jacob - Phys. Lett. 107B, 395 (1981).

53 - C. Gössling - private communication (1984).

54 - EMC Collaboration, J.J. Aubert et al. - Nucl. Phys. B213, 31 (1983).

55 - B.A. Campbell - Carleton Univ., Ottawa preprint (1981).

56 - V. Barger, F. Halzen and W.Y. Keung - Phys. Rev. D28, 1838 (1982).

57 - J. Ng and P. Zakarauskas - Phys. Rev. D29, 1838 (1982).

58 - Z. Kunszt - Bern University, preprint BUTP-84/10 (1984).

59 - R.N. Cahn and S. Dawson - Phys. Lett. 136B, 196 (1984), E 138B, 464 (1984).

60 - C. Jarlskog - private communication (1984).

61 - S.L. Glashow, D.V. Nanopoulos and A. Yildiz - Phys. Rev. D18, 1724 (1978).

62 - R.W. Brown and K.O. Mikaelian - Phys. Rev. D19, 922 (1979);
R.W. Brown, D. Sahdev and K.O. Mikaelian - Phys. Rev. D20, 1164 (1979).

63 - H.E. Haber and G.L. Kane - Nucl. Phys. B232, 333 (1984).

64 - UA1 COllaboration, G. Arnison et al. - Phys. Lett. 122B, 103 (1983).

65 - B.A. Campbell, J. Ellis and S. Rudaz - Nucl. Phys. B198, 1 (1982);
C. Kounnas and D.A. Ross - Nucl. Phs. B214, 317 (1983);
S.K. Jones and C.H. Llewellyn Smith - Nucl. Phys. B217, 145 (1983).

66 - I. Antoniadis, L. Baulieu and F. Delduc - Zeit. f. Phys. C23, 119 (1984)

67 - D. DiBitonto - private communication (1984).

68 - V. Barger, A.D. Martin and R.J.N. Phillips - Phys. Lett 125B, 339 (1983);
E. Berger, D. DiBitonto, M. Jacob and W.J. Stirling - CERN preprint TH-3821 (1984).

69 - W.J. Stirling - private communication (1984).

70 - R. Barbieri and L. Maiani - Pisa Univ. preprint IFUP TH 7/84 (1984).

71 - I.-H. Lee - Phys. Lett. 138B, 121 (1984).

72 - G.G. Ross and J. Valle - private communication (1984).

73 - J. Ellis, G. Gelmini, C. Jarlskog, G.G. Ross and J. Valle - in preparation (1984).

74 - P.F. Smith and J.R.J. Bennett - Nucl. Phys. B149, 525 (1979);
P.F. Smith et al. - Nucl. Phys. B206, 333 (1982).

75 - S. Dawson, E. Eichten and C. Quigg - FNAL preprint Pub-83/82 -THY/LBL-16540 (1984).

76 - S. Dimopoulos, S. Raby and G.L. Kane - Nucl. Phys. B182, 77 (1981).

77 - G. Girardi, P. Méry and P. Sorba - Nucl. Phys. B195, 410 (1982).

Figure Captions

1 - Tree level scattering cross-sections (a) should fall as $1/E_{cm}^2$ at high energies, if loop diagrams (b) are not to be unrenormalizably divergent [14].

2 - The tree-level diagrams for $f\bar{f} \to$ gauge boson pairs in a non-abelian gauge theory.

3 - The necessary correction diagrams due to the exchange of something like a Higgs boson.

4 - The decay width Γ_H of a heavy Higgs [19] into W^+W^-, $Z^\circ Z^\circ$ and $\bar{t}t$, assuming m_t = 30 GeV. Also shown are lines corresponding to $\Gamma_H = (10^{-2}, 10^{-1})\ m_H$.

5 - (a) Loop corrections to the Higgs mass, due to fermions, vector bosons, and scalar bosons. (b) Scalar boson propagating through space-time foam [24].

6 - The generic model for producting a new massive state though a generalization of the Drell-Yan [42] mechanism.

7 - Effective parton-parton luminosity functions plotted in terms of $\sqrt{\tau}$. They do not vary much between $\sqrt{s}$ = 10 and 40 TeV. Note the similarity of the luminosities in pp and $p\bar{p}$ collisions for $\sqrt{\tau} \leq 0.1$ corresponding to $m_X \leq \frac{1}{10}\sqrt{s}$.

8 - Some of the parton-parton luminosity functions of fig.7 multiplied by a geometrical cross-section factor $1/m_X^2$ (3.5). The horizontal dashed (dotted) lines correspond to σ=0 ($\frac{1}{10}$) pb above which cross-sections should be observable with a hadron-hadron luminosity of $10^{32}(10^{33})\text{cm}^{-2}\text{sec}^{-1}$.

9 - Rapidity distribution [49] for $pp \to W^+ + x$ at E_{cm} = 40 TeV.

10 - The angle of archaeology: today's physics emerges at wide angles, yesterday's physics emerges closer to the beam pipe, last week's physics even closer, etc.

11 - Double-subprocess [22] due to two simultaneous hard collisions analogous to that in fig.6 occuring in the same event.

12 - Quark loop diagram [51] for $gg \to H$.

13 - Cross-sections for $gg \to H$ at $\sqrt{s}$ = 10 TeV, 20 TeV and 40 TeV, evaluated with m_t = 35, 70 and 100 GeV.

14 - The rapidity distribution of the Higgs decay products for different values of m_H.

15 - Examples of Higgs bremsstrahlung diagrams [57,58] for $gg \to t\bar{t}H$ and $\bar{q}q \to t\bar{t}H$.

16 - Cross-sections for $\bar{t}tH$ production for $\sqrt{s}$ = 10, 20, 40 TeV and m_t = 35 GeV.

17 - Final state distributions for $\bar{t}tH$ production with m_H = 200 GeV at $\sqrt{s}$ = 20 TeV:

(a) rapidity distribution of the Higgs,

(b) rapidity distribution of the $t(\bar{t})$ quark,

(c) p_T distribution of the Higgs,

(d) p_T distribution of the t $(\bar{t})$ quark,

(e) invariant mass for the $(\bar{t}t)$ system.

18 - Diagram for $WW \to H$ production [59] in qq, $q\bar{q}$ or $\bar{q}\bar{q}$ scattering.

19 - Cross-sections for $WW \to H$ production.

20 - Distribution in the subprocess centre-of-mass rapidity $\hat{y}$ for Higgses in WW collisions [60]. Note the flat distribution which builds up the logarithm in equation (3.16).

21 - Diagram for $\bar{q}q \to W^* \to W+H$ production [61].

22 - Cross- sections for $\bar{q}q \to W^* \to W+H$ production.

23 - A compilation of Higgs production cross-sections in $p\bar{p}$ collisions at $\sqrt{s}$ = 20 TeV.

24 - Total cross-section for $\bar{t}t$ production, to be considered as a background to searches for Higgses or technipions P_8.

25 - The cross-sections for $(\bar{t}t\bar{t}t)$ production and $(\bar{t}tH)$ production [58].

26 - Final state distributions [58] for $(\bar{t}t\bar{t}t)$ production: (a) the rapidity distribution for a $(\bar{t}t)$ pair, (b) the invariant mass of a $(\bar{t}t)$ pair (note the peaking at $m_{\bar{t}t} < 2m_W$, just where we would want to look for the Higgs), (c) p_T distributions for t quarks and for $(\bar{t}t)$ pairs. Note the similarities between these distributions and those given for $(\bar{t}tH)$ production in fig.17.

27 - Total cross sections for W^+W^- and $Z^\circ Z^\circ$ production [62] in pp and $p\bar{p}$ collisions, as functions of $\sqrt{s}$.

28 - Invariant mass distributions for W^+W^- and $Z^\circ Z^\circ$ pairs produced by $\bar{q}q$ annihilation.

29 -Angular distributions (a) for W^+W^-, and (b) for $Z^\circ Z^\circ$ production at different values of $\sqrt{\hat{s}}$.

30 - Cross-sections for $\tilde{g}\tilde{g}$ production [39], indicating the sensitivity to $m_{\tilde{q}}$.

31 - The missing p_T signature from $\tilde{g}\tilde{g}$ production followed by $\tilde{g} \to q + \bar{q} + \tilde{\gamma}$ decay.

32 - Cross-sections for $\tilde{g}\tilde{g}$ production followed by $\tilde{g} \to q + \bar{q} + \tilde{\gamma}$ decay giving final states with $p_T^{miss} > 4_\sigma$ as defined in equation (3.25).

33 - Rapidity distribution for q and $\bar{q}$ jets from $\tilde{g}\tilde{g}$ production followed by $\tilde{g} \to q + \bar{q} + \tilde{\gamma}$ decay.

34 - The distribution of the p_T of the minimum p_T jet from $\tilde{g}\tilde{g}$ production followed by $q\bar{q}\tilde{\gamma}$ decay.

35 - Cross-sections for $\tilde{q}\bar{\tilde{q}}$ production [39], indicating the sensitivity to $m_{\tilde{g}}$.

36 - The missing P_T signature from $\tilde{q}\bar{\tilde{q}}$ production followed by (a) $\tilde{q} \to q + \tilde{g}$ decay (b) $\tilde{q} \to q + \tilde{\gamma}$ decay.

37 - Cross-sections for $\tilde{q}\bar{\tilde{q}}$ production followed by $\tilde{q} \to q + \tilde{g}$ decay, giving final states with $P_T^{miss} > 4\sigma$ as defined in equation (3.25).

38 - The rapidity distribution for q and $\bar{q}$ jets from $\tilde{q}\bar{\tilde{q}}$ production followed by (a) $\tilde{q} \to q + \tilde{g}$, $\tilde{g} \to q + \bar{q} + \tilde{\gamma}$, (b) $\tilde{q} \to q + \tilde{\gamma}$.

39 - The distribution of the P_T of the minimum P_T jet from $\tilde{q}\bar{\tilde{q}}$ production followed by $\tilde{q} \to q + \tilde{g}$, $\tilde{g} \to q + \bar{q} + \tilde{\gamma}$ decay.

40 - Distribution in the scaled minimum transverse mass [68] $\xi \equiv m^*/m_{\tilde{g}}$ for diffractive $\tilde{g}\tilde{g}$ production. The sharp peak comes from correctly paired jets, while the broad distribution comes from wrong combinations.

41 - Distribution in p_T^{miss} transverse to the nearest final state jet axis (a) for $\tilde{g}\tilde{g}$, $\tilde{g} \to q + \bar{q} + \tilde{\gamma}$ decay.

42 - Cross-sections for coloured technipion P_8, coloured technivector V_8 and techniquark continuum $Q_T Q_T$ production.

43 - Sharply peaked centre-of-mass angular distribution for $\tilde{g}\tilde{g} \to t\bar{t}$, to be compared with the isotropic distribution from $P_8 \to \bar{t}t$ decay.

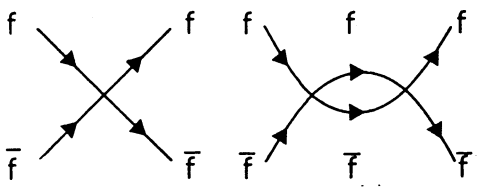

Fig. 1

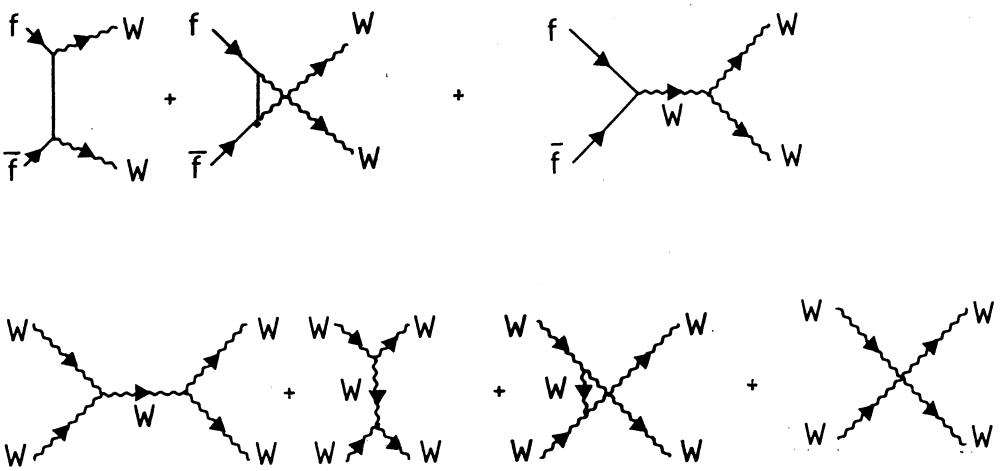

Fig. 2

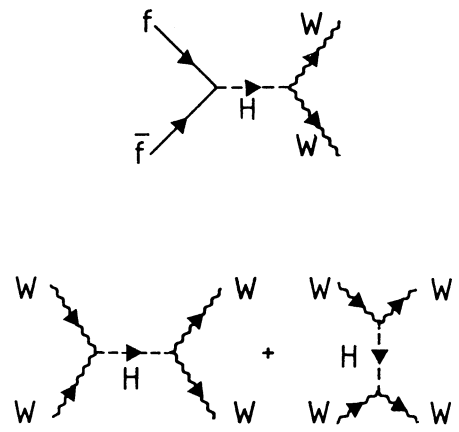

Fig. 3

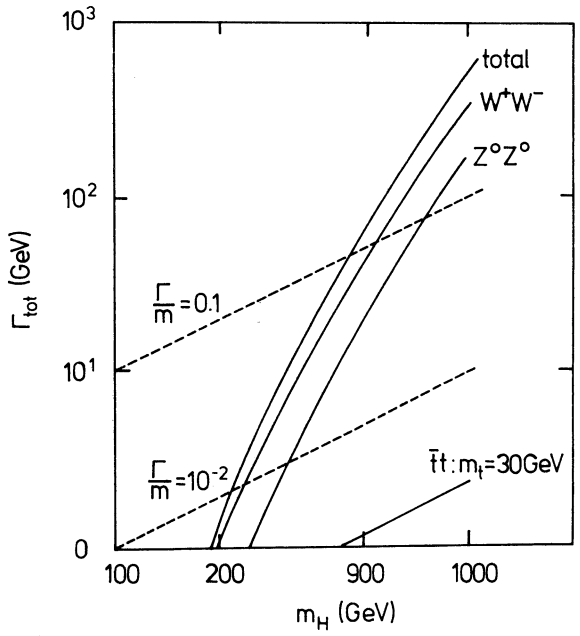

Fig. 4

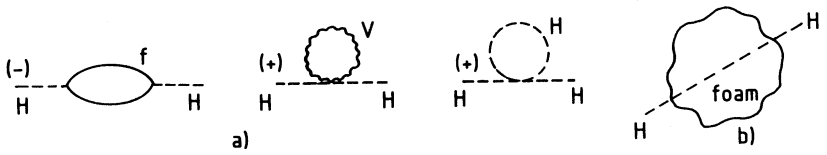

Fig. 5

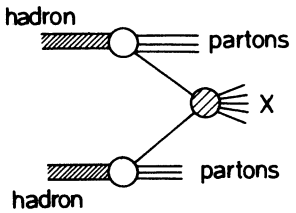

Fig. 6

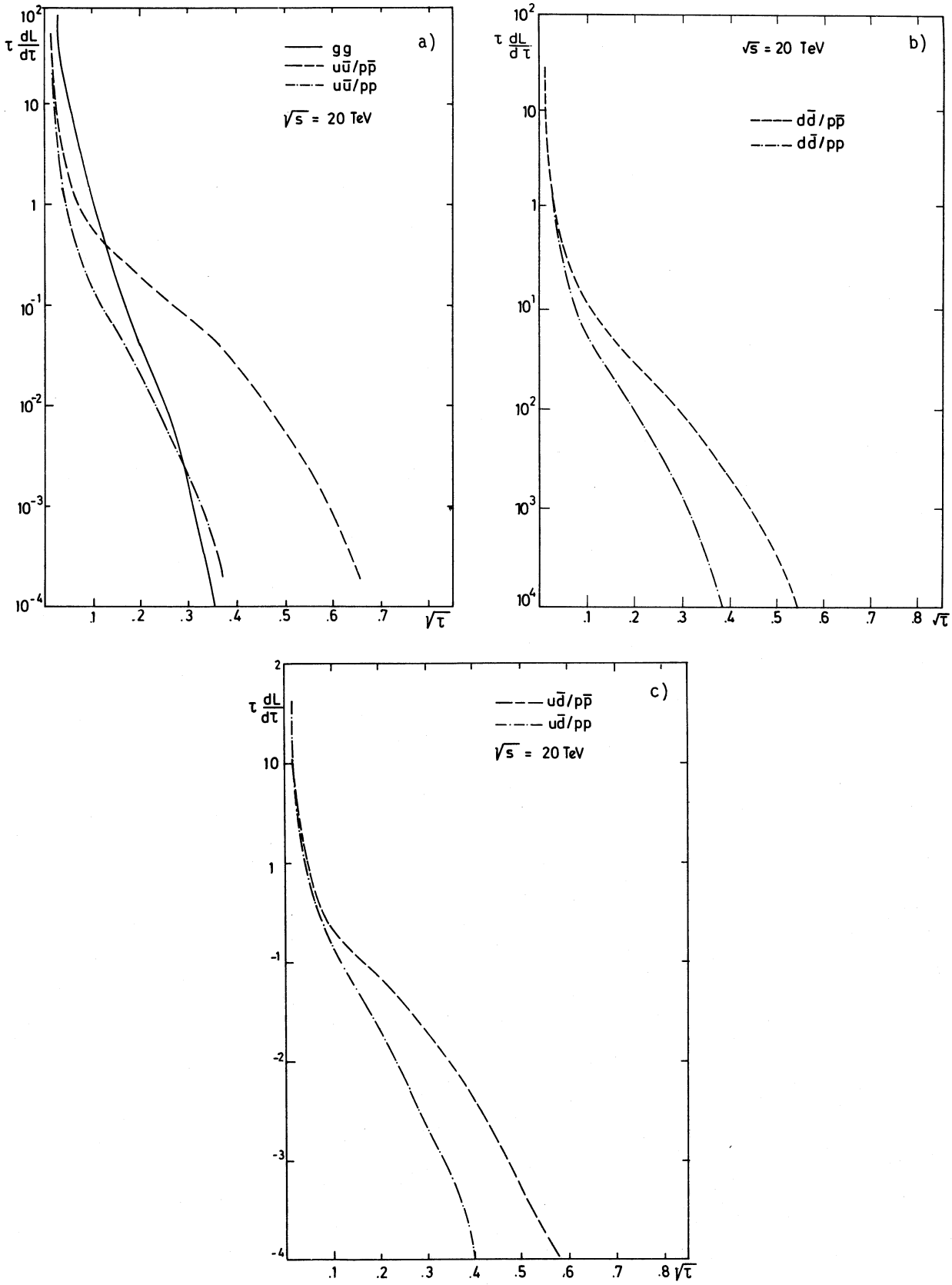
a)
gg
uū/pp̄
uū/pp
√s = 20 TeV
τ dL/dτ
√τ
b)
√s = 20 TeV
dd̄/pp̄
dd̄/pp
c)
ud̄/pp̄
ud̄/pp
√s = 20 TeV

Fig. 7

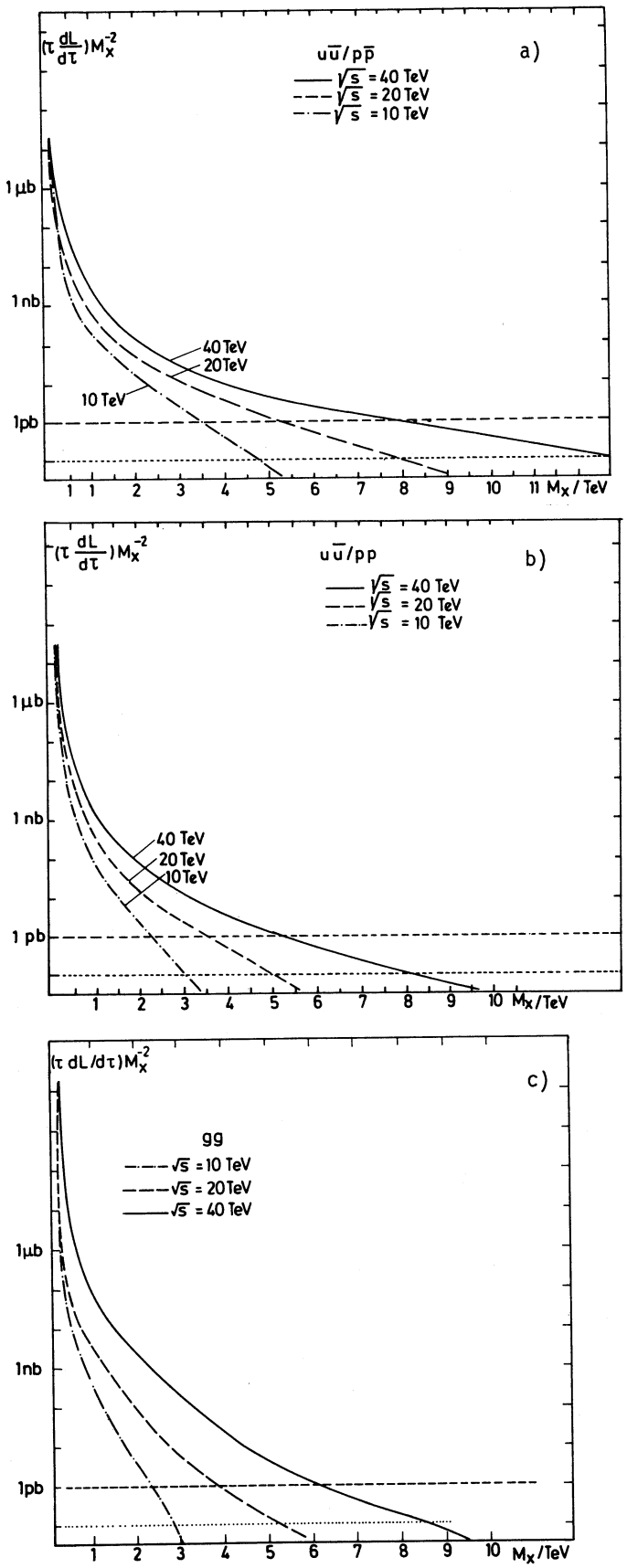
$(\tau \frac{dL}{d\tau}) M_x^{-2}$
$u\bar{u}/p\bar{p}$
a)
$\sqrt{s}$ = 40 TeV
$\sqrt{s}$ = 20 TeV
$\sqrt{s}$ = 10 TeV
1 μb
1 nb
1 pb
40 TeV
20 TeV
10 TeV
1 1 2 3 4 5 6 7 8 9 10 11 M_x / TeV
$(\tau \frac{dL}{d\tau}) M_x^{-2}$
$u\bar{u}/pp$
b)
$\sqrt{s}$ = 40 TeV
$\sqrt{s}$ = 20 TeV
$\sqrt{s}$ = 10 TeV
1 μb
1 nb
1 pb
40 TeV
20 TeV
10 TeV
1 2 3 4 5 6 7 8 9 10 M_x/TeV
$(\tau\, dL/d\tau) M_x^{-2}$
c)
gg
$\sqrt{s}$ = 10 TeV
$\sqrt{s}$ = 20 TeV
$\sqrt{s}$ = 40 TeV
1μb
1nb
1pb
1 2 3 4 5 6 7 8 9 10 M_x/TeV

Fig. 8

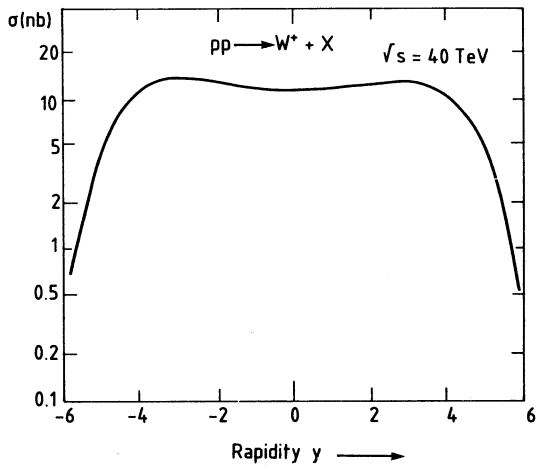

Fig. 9

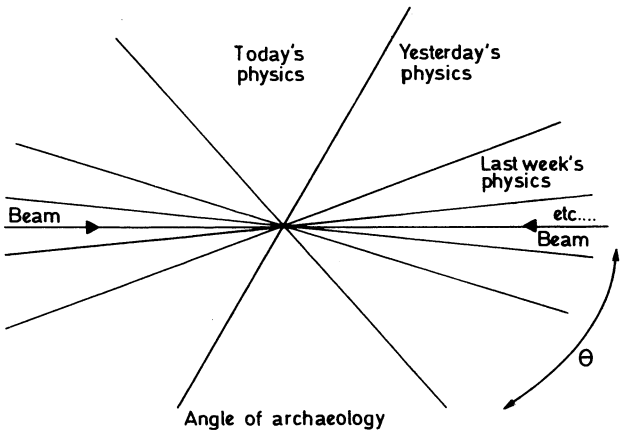

Fig. 10

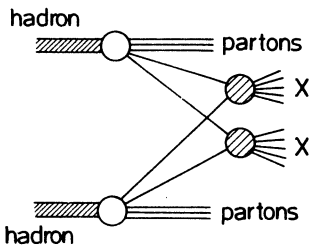

Fig. 11

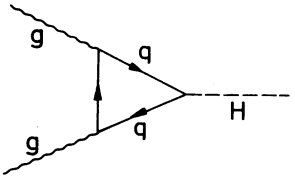

Fig. 12

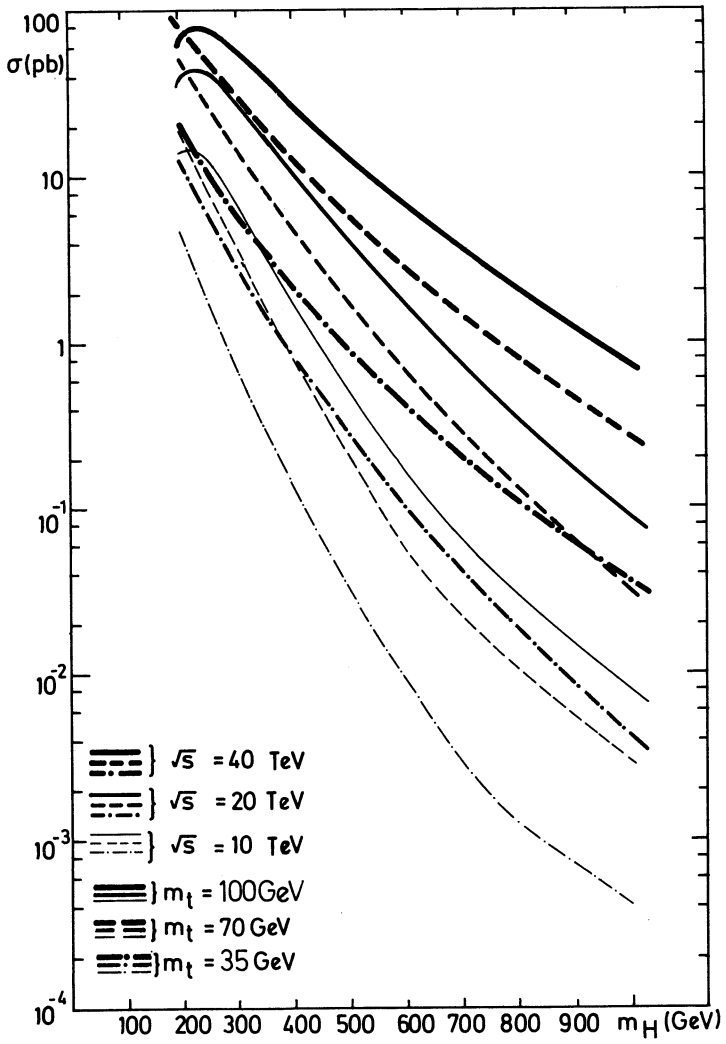
100
σ(pb)
10
1
10^-1
10^-2
10^-3
10^-4
100 200 300 400 500 600 700 800 900 m_H (GeV)
√s = 40 TeV
√s = 20 TeV
√s = 10 TeV
m_t = 100GeV
m_t = 70 GeV
m_t = 35 GeV

Fig. 13

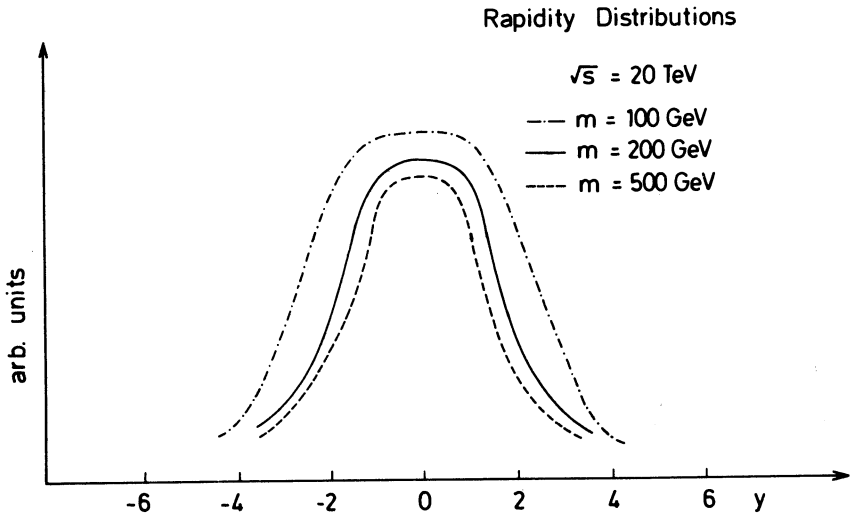
Rapidity Distributions
√s = 20 TeV
m = 100 GeV
m = 200 GeV
m = 500 GeV
arb. units
-6 -4 -2 0 2 4 6 y

Fig. 14

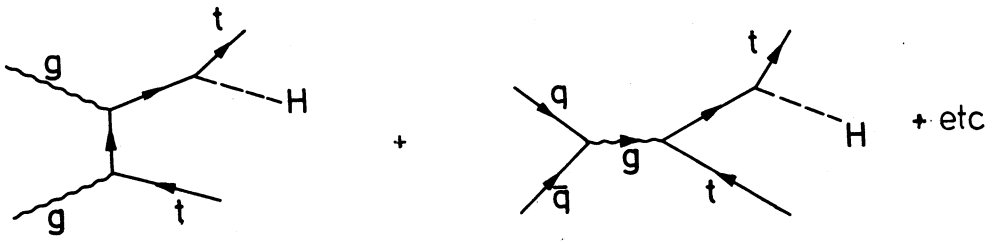
g
t
H
g
t
+
q
t
H
g
q̄
t
+ etc

Fig. 15

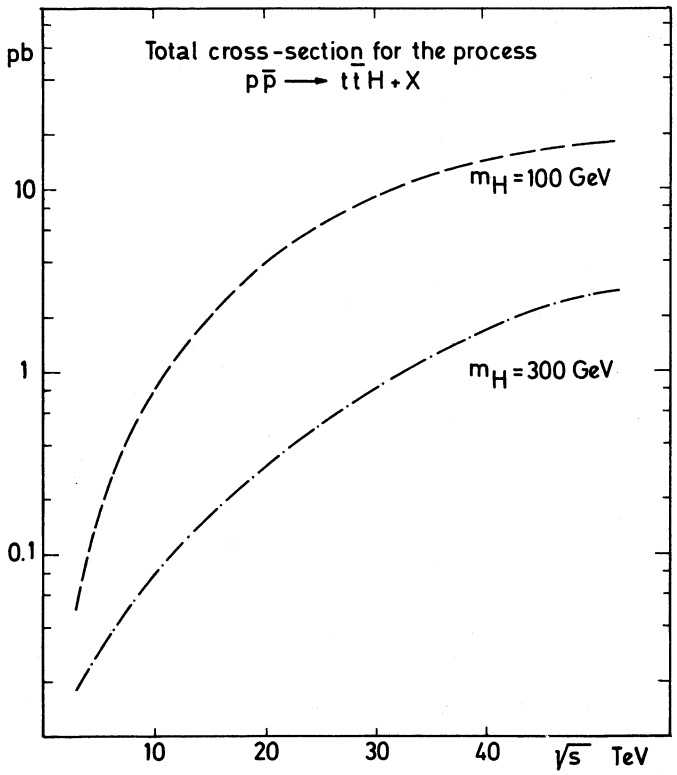
Total cross-section for the process
$p\bar{p} \longrightarrow t\bar{t}H+X$
pb
10
1
0.1
m_H=100 GeV
m_H=300 GeV
10
20
30
40
$\sqrt{s}$ TeV

Fig. 16

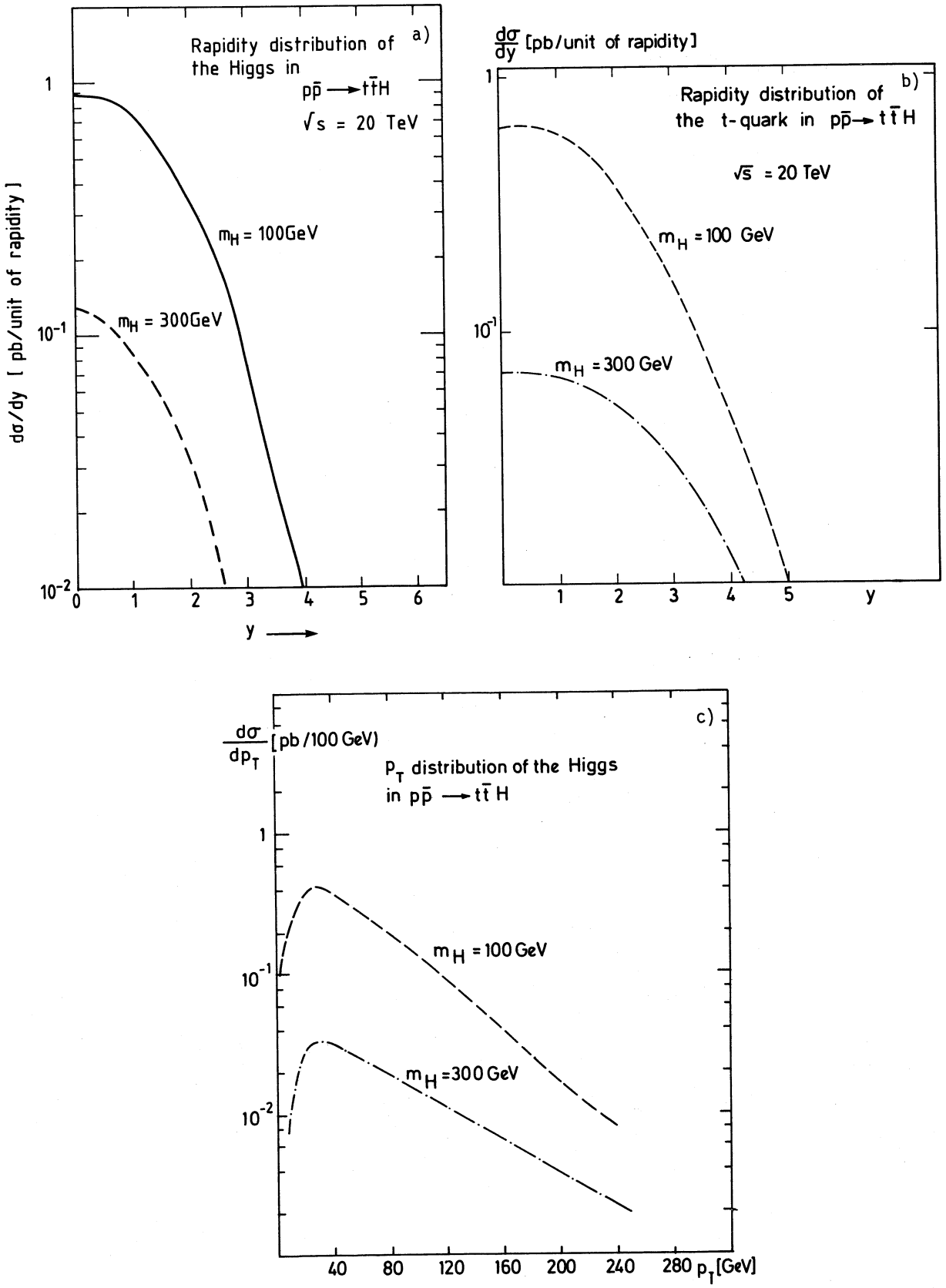
a)
Rapidity distribution of the Higgs in
pp̄ → tt̄H
√s = 20 TeV
m_H = 100GeV
m_H = 300GeV
dσ/dy [pb/unit of rapidity]
y
b)
Rapidity distribution of the t-quark in pp̄ → tt̄H
√s = 20 TeV
m_H = 100 GeV
m_H = 300 GeV
dσ/dy [pb/unit of rapidity]
y
c)
dσ/dp_T [pb/100 GeV]
p_T distribution of the Higgs in pp̄ → tt̄H
m_H = 100 GeV
m_H = 300 GeV
p_T [GeV]

Fig. 17

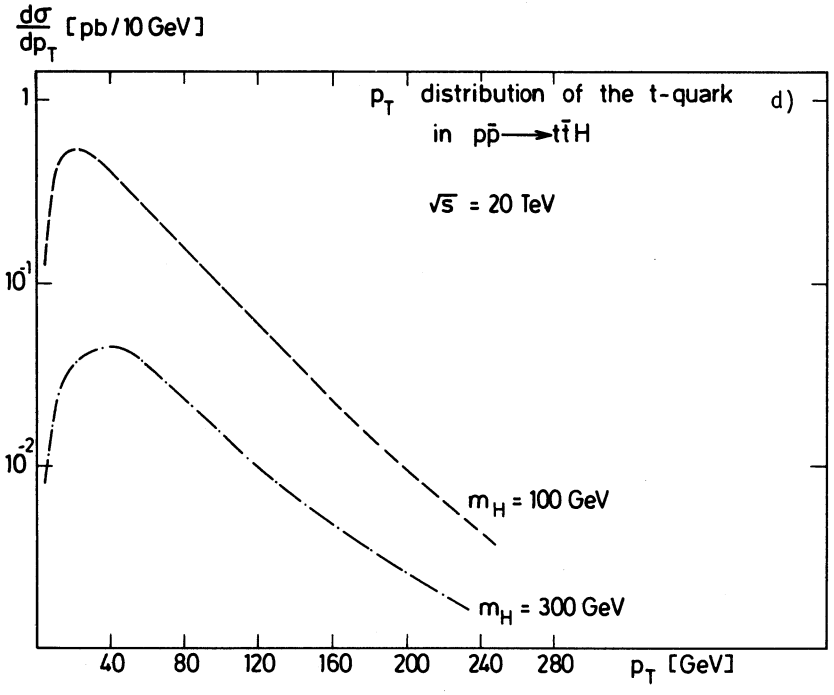
dσ/dp_T [pb/10 GeV]
1
10^-1
10^-2
p_T distribution of the t-quark d)
in pp̄ → tt̄H
√s = 20 TeV
m_H = 100 GeV
m_H = 300 GeV
40 80 120 160 200 240 280
p_T [GeV]

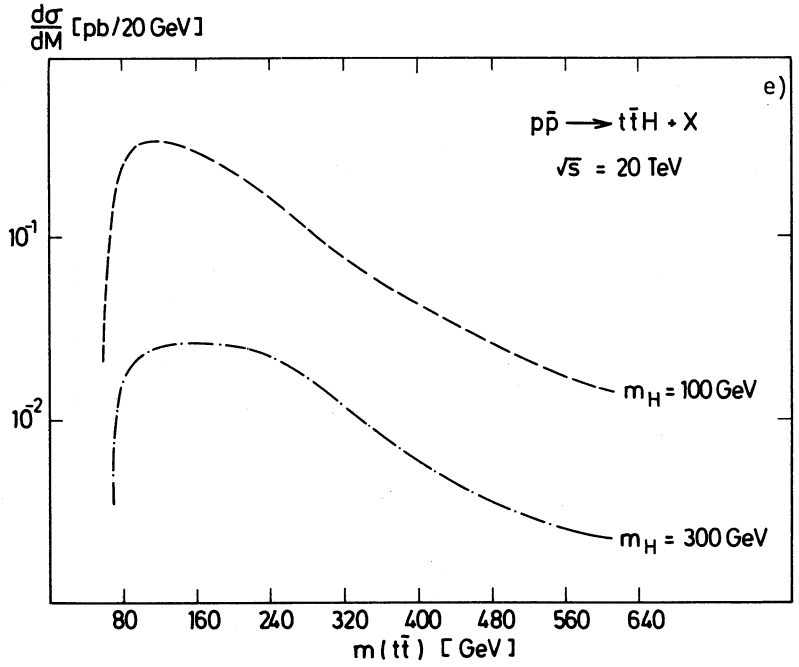
dσ/dM [pb/20 GeV]
e)
pp̄ → tt̄H + X
√s = 20 TeV
10^-1
10^-2
m_H = 100 GeV
m_H = 300 GeV
80 160 240 320 400 480 560 640
m(tt̄) [GeV]

Fig. 17

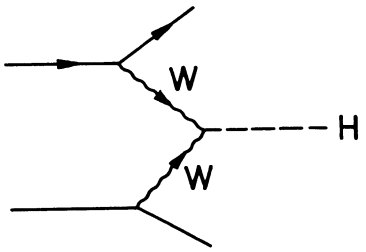

Fig. 18

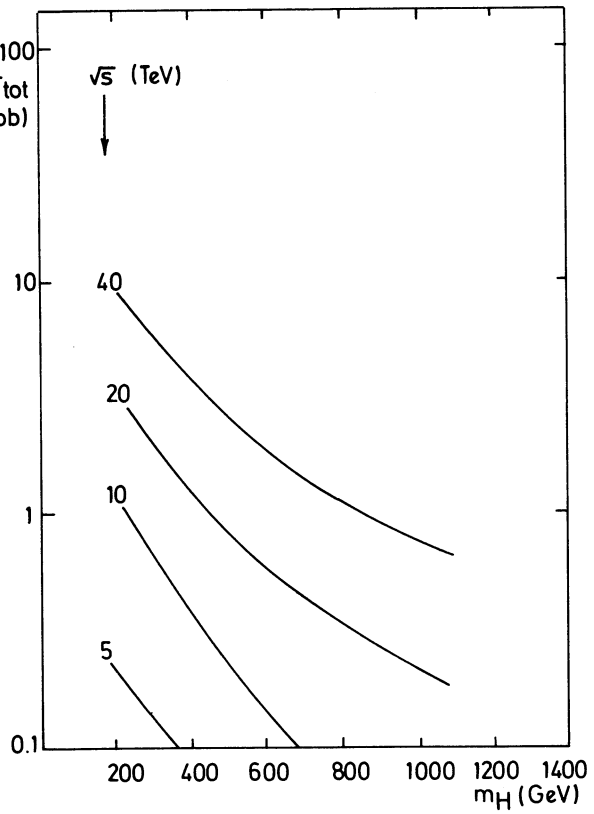

Fig. 19

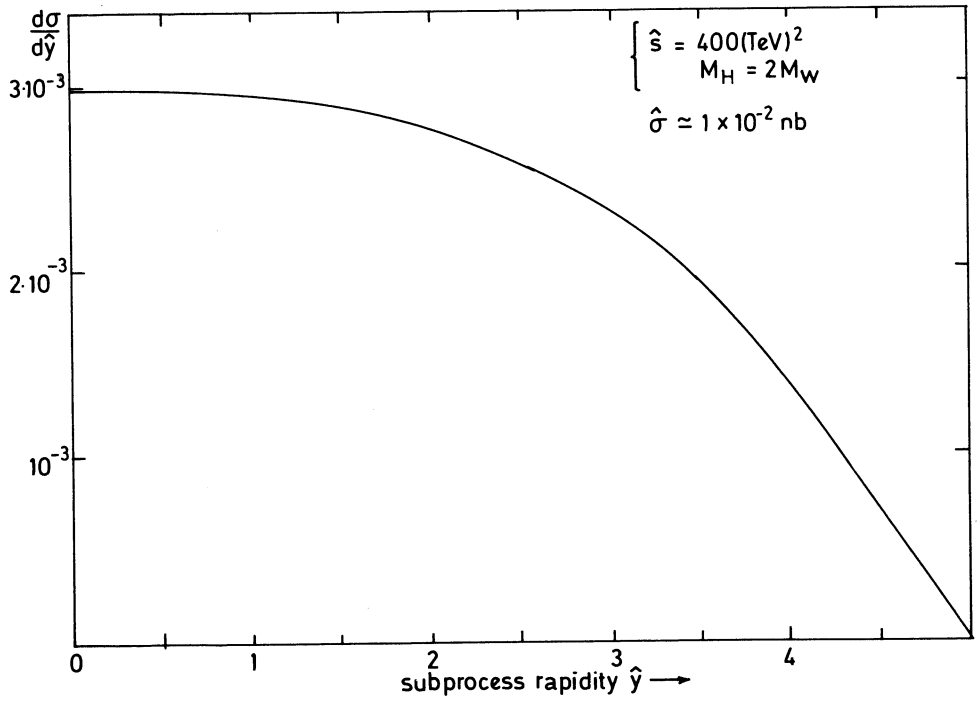

Fig. 20

Fig. 21

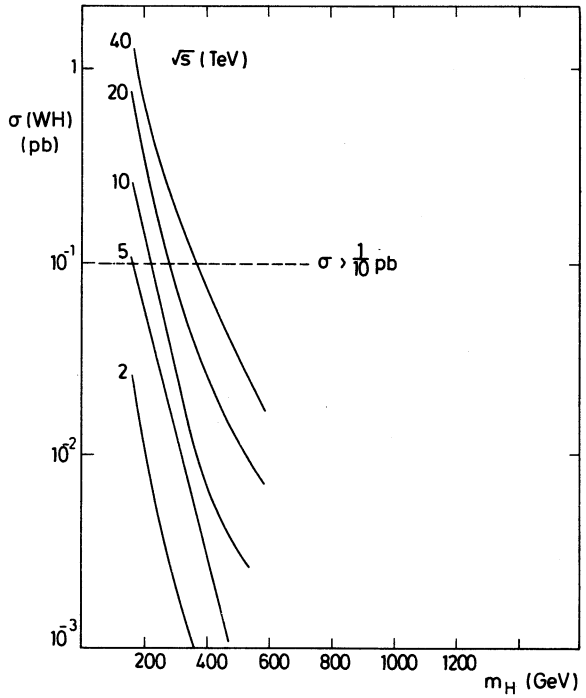

Fig. 22

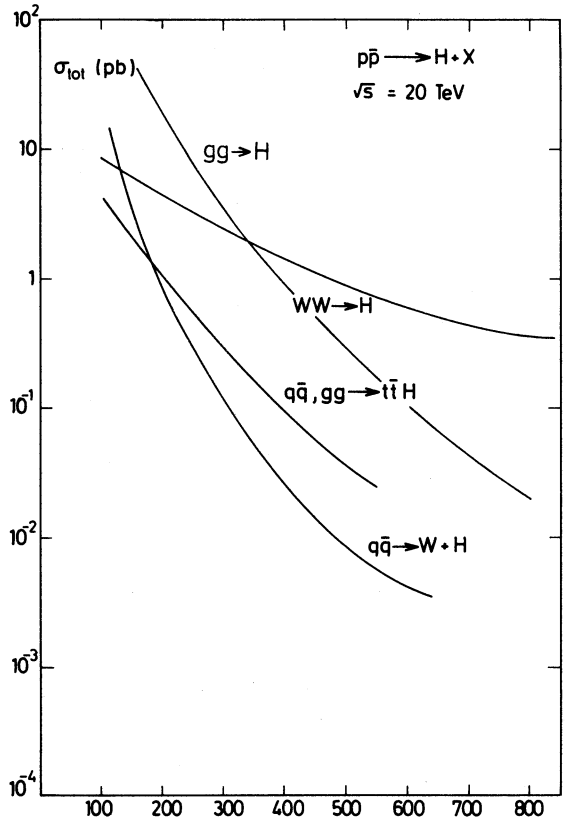

Fig. 23

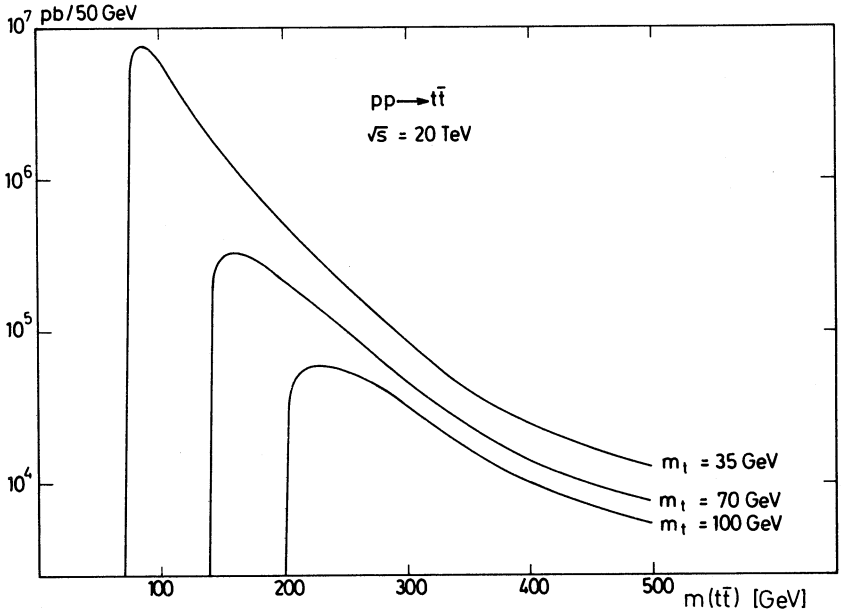
10^7 pb/50 GeV
$pp \rightarrow t\bar{t}$
$\sqrt{s}$ = 20 TeV
10^6
10^5
10^4
m_t = 35 GeV
m_t = 70 GeV
m_t = 100 GeV
100
200
300
400
500
$m(t\bar{t})$ [GeV]

Fig. 24

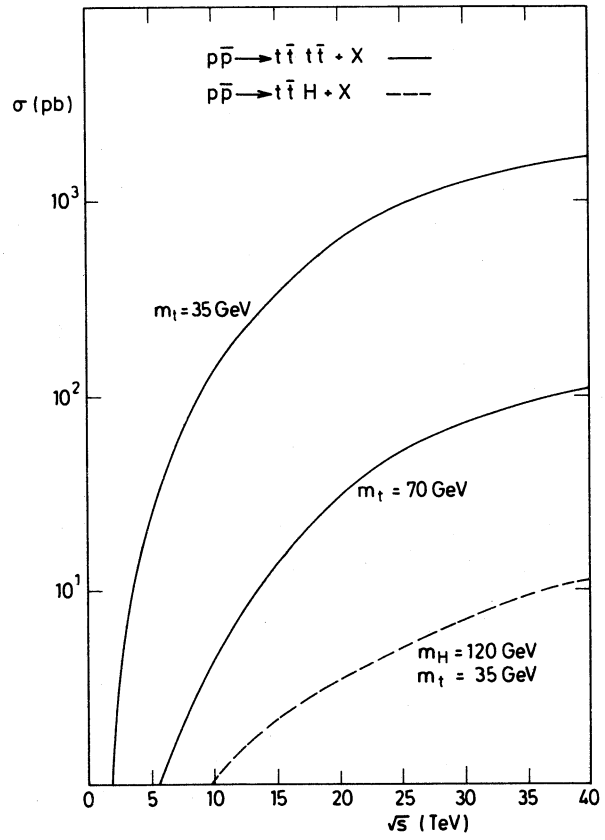
$p\bar{p} \rightarrow t\bar{t}\,t\bar{t} + X$
$p\bar{p} \rightarrow t\bar{t}\,H + X$
σ (pb)
10^3
10^2
10^1
m_t = 35 GeV
m_t = 70 GeV
m_H = 120 GeV
m_t = 35 GeV
0
5
10
15
20
25
30
35
40
$\sqrt{s}$ (TeV)

Fig. 25

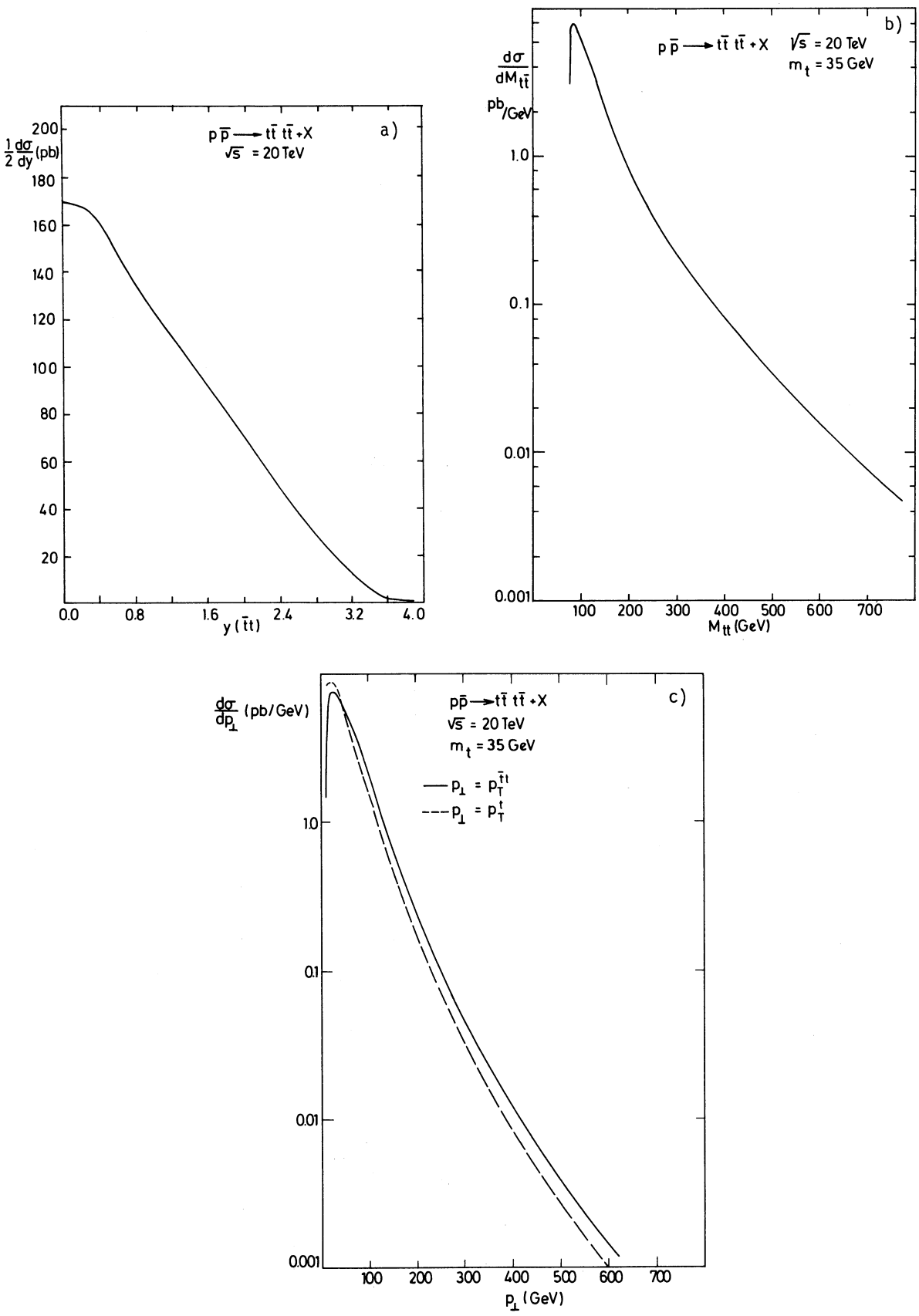
a)
$p\bar{p} \to t\bar{t}\,t\bar{t} + X$
$\sqrt{s}$ = 20 TeV
$\frac{1}{2}\frac{d\sigma}{dy}$ (pb)
200
180
160
140
120
100
80
60
40
20
0.0
0.8
1.6
2.4
3.2
4.0
y ($t\bar{t}$)
b)
$p\bar{p} \to t\bar{t}\,t\bar{t} + X$
$\sqrt{s}$ = 20 TeV
m_t = 35 GeV
$\frac{d\sigma}{dM_{t\bar{t}}}$
pb/GeV
1.0
0.1
0.01
0.001
100
200
300
400
500
600
700
M_{tt} (GeV)
c)
$p\bar{p} \to t\bar{t}\,t\bar{t} + X$
$\sqrt{s}$ = 20 TeV
m_t = 35 GeV
$p_\perp = p_T^{t\bar{t}}$
$p_\perp = p_T^{t}$
$\frac{d\sigma}{dp_\perp}$ (pb/GeV)
1.0
0.1
0.01
0.001
100
200
300
400
500
600
700
$p_\perp$ (GeV)

Fig. 26

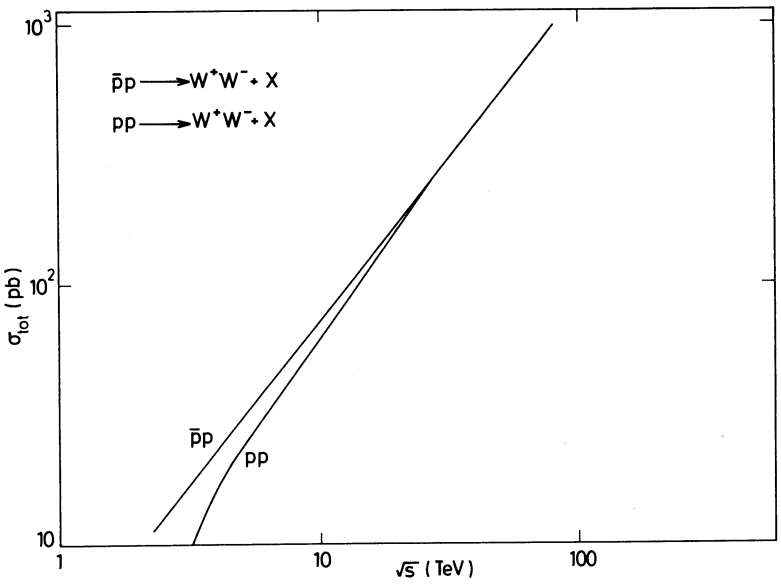
10^3
10^2
10
σ_{tot} (pb)
$\bar{p}p \longrightarrow W^+W^- + X$
$pp \longrightarrow W^+W^- + X$
$\bar{p}p$
pp
1
10
100
$\sqrt{s}$ (TeV)

Fig. 27

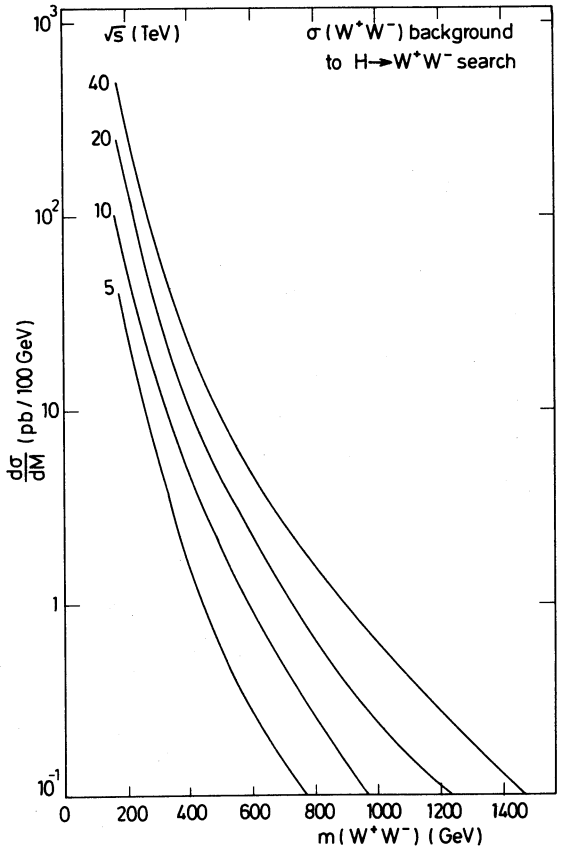
10^3
10^2
10
1
10^{-1}
$\frac{d\sigma}{dM}$ (pb / 100 GeV)
$\sqrt{s}$ (TeV)
40
20
10
5
$\sigma(W^+W^-)$ background
to $H \rightarrow W^+W^-$ search
0
200
400
600
800
1000
1200
1400
$m(W^+W^-)$ (GeV)

Fig. 28

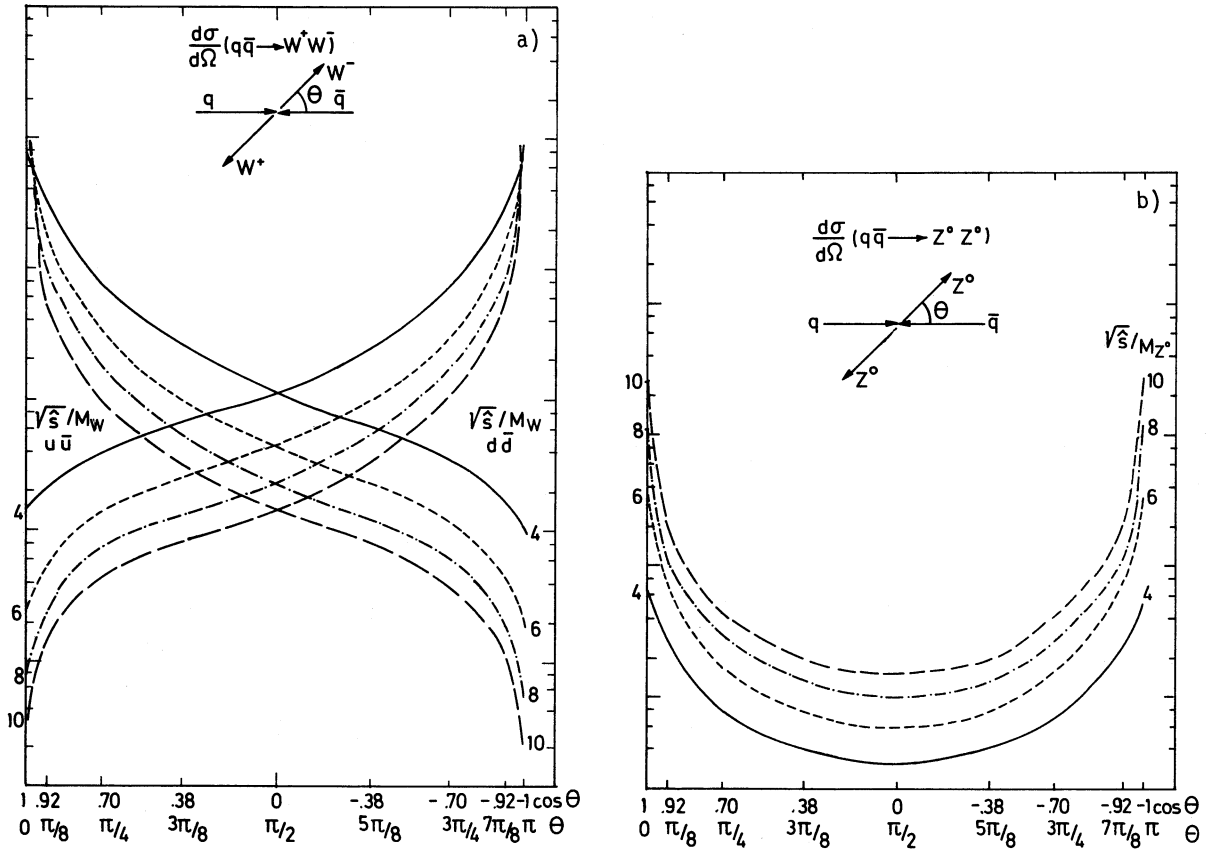
a)
$\frac{d\sigma}{d\Omega}(q\bar{q}\to W^+W^-)$
q
θ
$\bar{q}$
W^-
W^+
$\sqrt{\hat{s}}/M_W$
u ū
$\sqrt{\hat{s}}/M_W$
d d̄
4
6
8
10
1 .92 .70 .38 0 -.38 -.70 -.92 -1 cos Θ
0 π/8 π/4 3π/8 π/2 5π/8 3π/4 7π/8 π Θ
b)
$\frac{d\sigma}{d\Omega}(q\bar{q}\to Z^\circ Z^\circ)$
q
θ
$\bar{q}$
Z°
Z°
$\sqrt{\hat{s}}/M_{Z^\circ}$
10
8
6
4
1 .92 .70 .38 0 -.38 -.70 -.92 -1 cos Θ
0 π/8 π/4 3π/8 π/2 5π/8 3π/4 7π/8 π Θ

Fig. 29

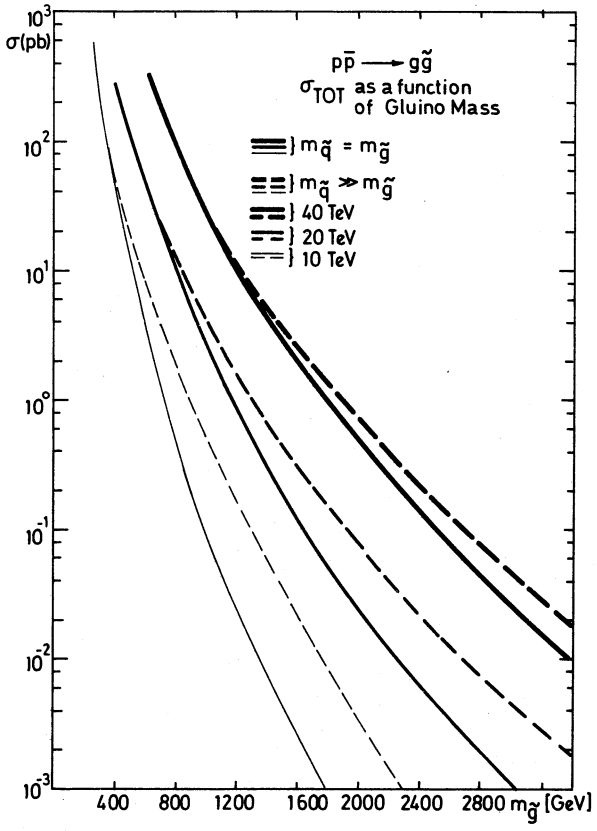
σ(pb)
10^3
10^2
10^1
10^0
10^{-1}
10^{-2}
10^{-3}
$p\bar{p}\to g\tilde{g}$
σ_{TOT} as a function of Gluino Mass
$m_{\tilde{q}} = m_{\tilde{g}}$
$m_{\tilde{q}} \gg m_{\tilde{g}}$
40 TeV
20 TeV
10 TeV
400 800 1200 1600 2000 2400 2800 $m_{\tilde{g}}$ [GeV]

Fig. 30

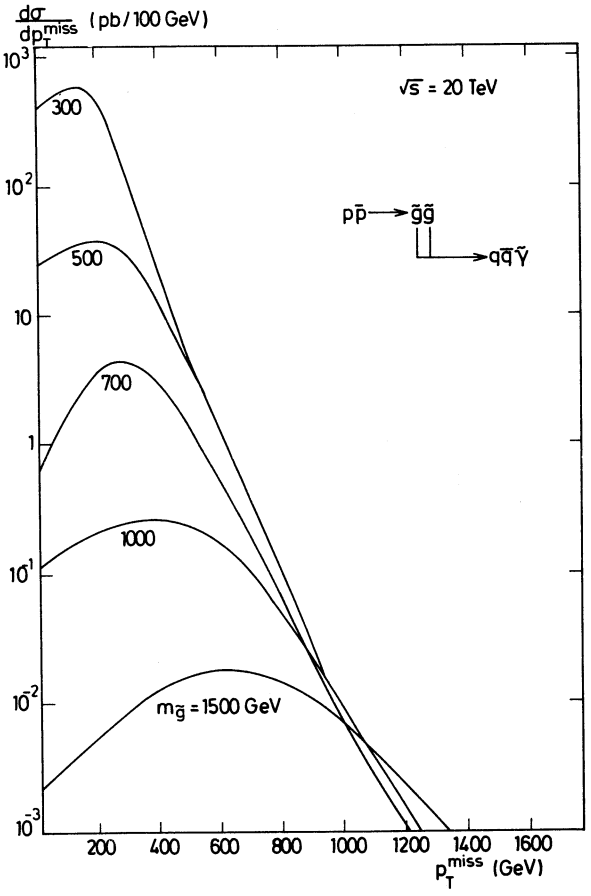

Fig. 31

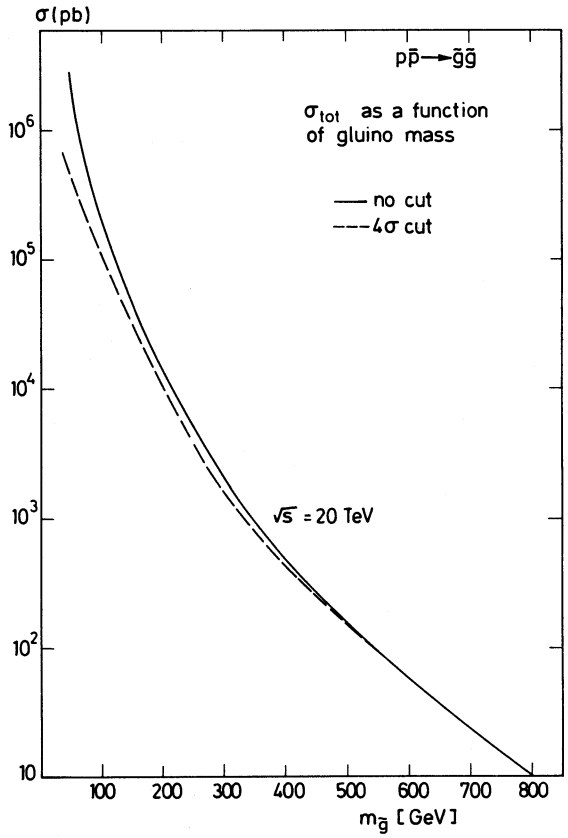

Fig. 32

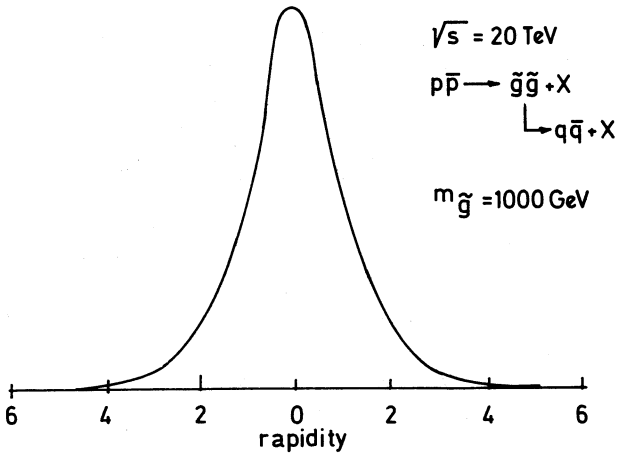

Fig. 33

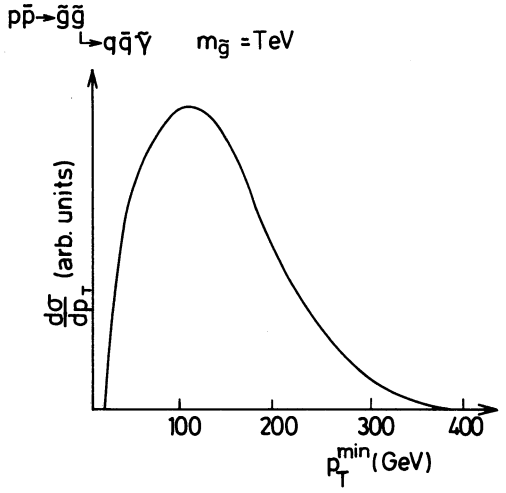
pp̄→g̃g̃
↳qq̄γ̃
m_g̃ =TeV
dσ/dp_T (arb. units)
100
200
300
400
p_T^min (GeV)

Fig. 34

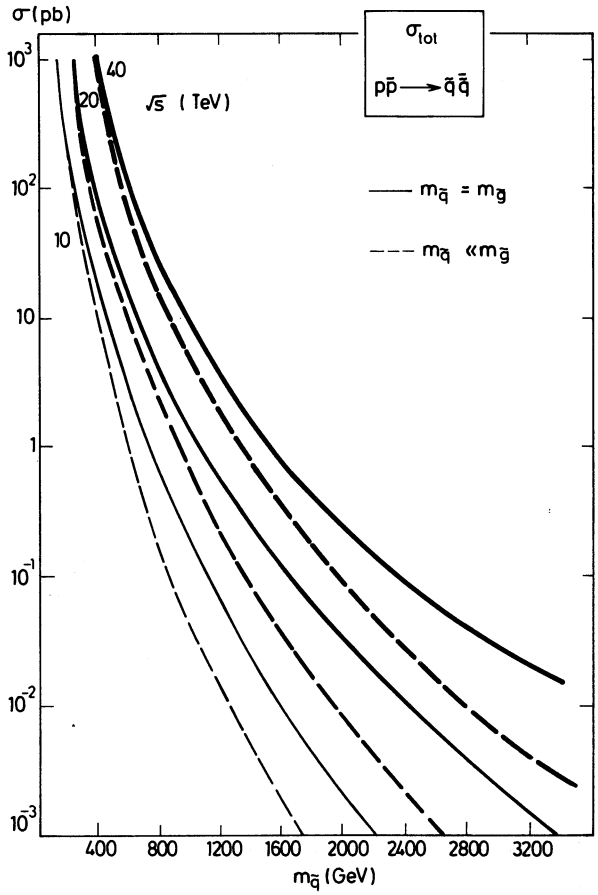
σ(pb)
σ_tot
pp̄ → q̃q̃
√s (TeV)
40
20
10
m_q̃ = m_g̃
m_q̃ « m_g̃
10^3
10^2
10
1
10^-1
10^-2
10^-3
400
800
1200
1600
2000
2400
2800
3200
m_q̃ (GeV)

Fig. 35

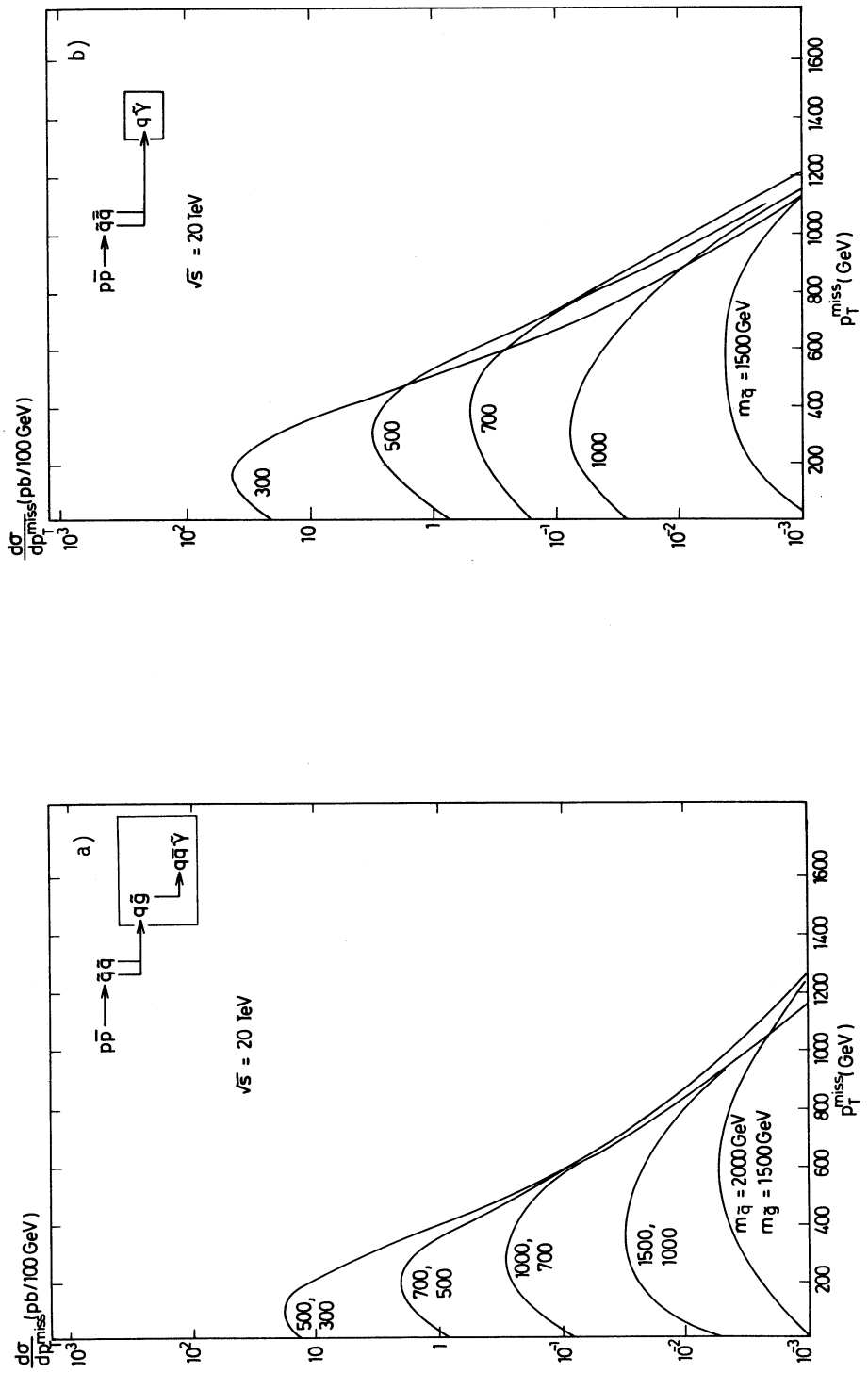
a)
$p\bar{p} \to \tilde{q}\bar{\tilde{q}}$
$q\tilde{g}$
$q\bar{q}\tilde{\gamma}$
$\sqrt{s}$ = 20 TeV
500, 300
700, 500
1000, 700
1500, 1000
$m_{\tilde{q}}$ = 2000 GeV
$m_{\tilde{g}}$ = 1500 GeV
$\frac{d\sigma}{dp_T^{miss}}$ (pb/100 GeV)
p_T^{miss} (GeV)
b)
$p\bar{p} \to \tilde{q}\bar{\tilde{q}}$
$q\tilde{\gamma}$
$\sqrt{s}$ = 20 TeV
300
500
700
1000
$m_{\tilde{q}}$ = 1500 GeV
$\frac{d\sigma}{dp_T^{miss}}$ (pb/100 GeV)
p_T^{miss} (GeV)

Fig. 36

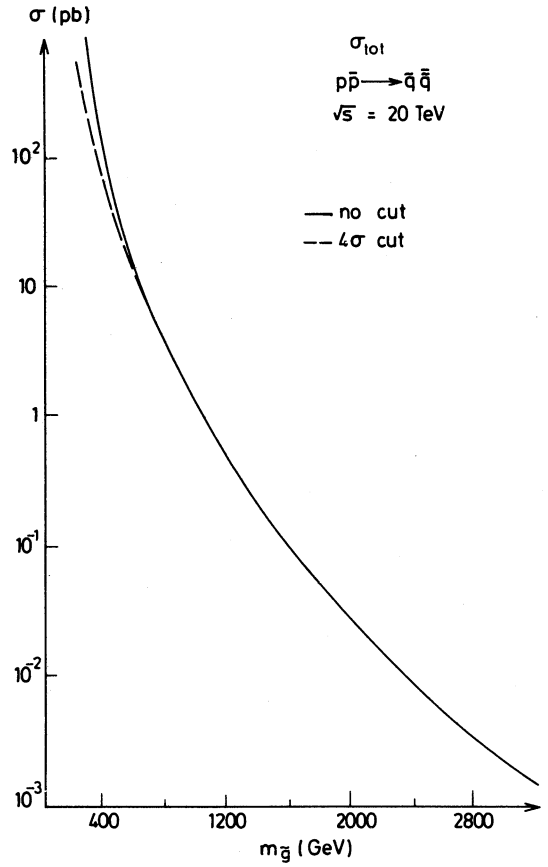

Fig. 37

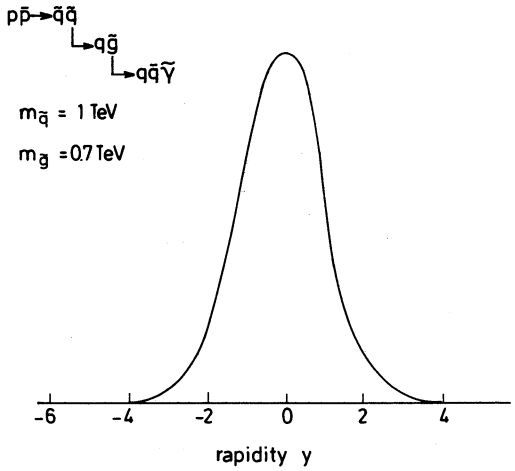

Fig. 38

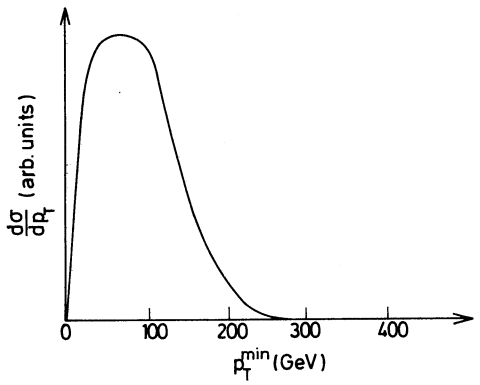

Fig. 39

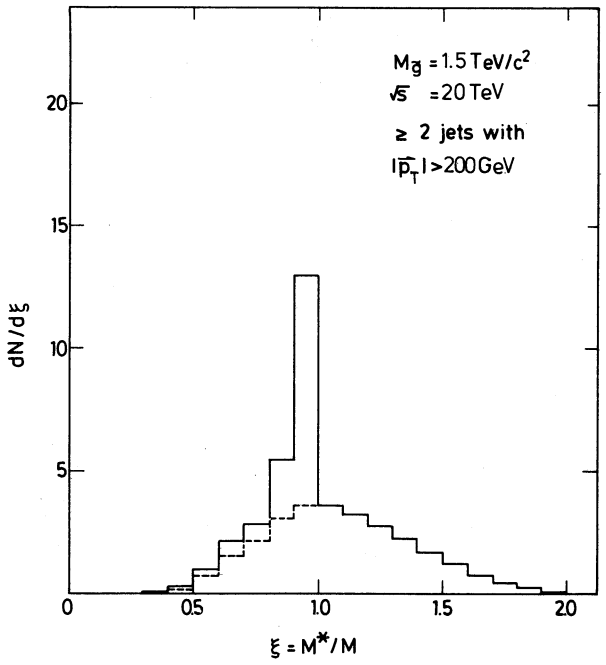

Fig. 40

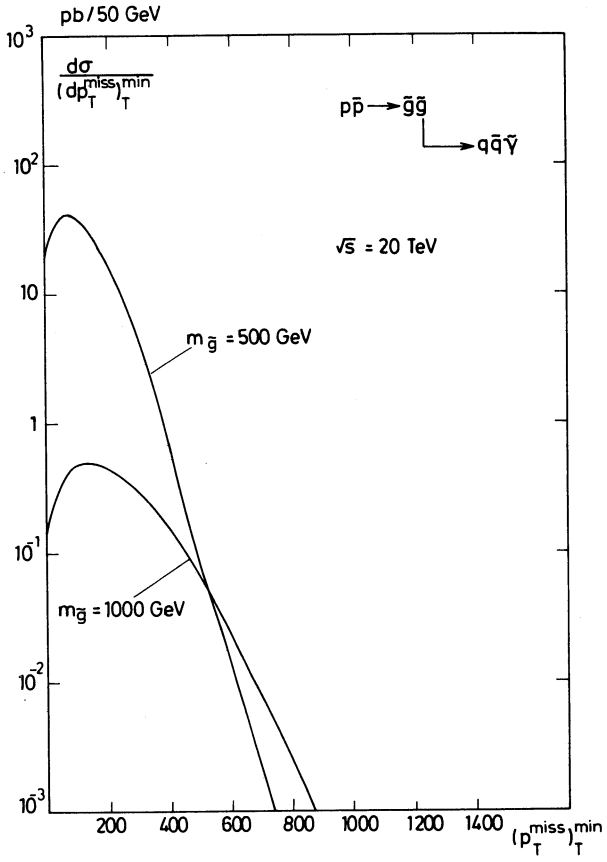

Fig. 41

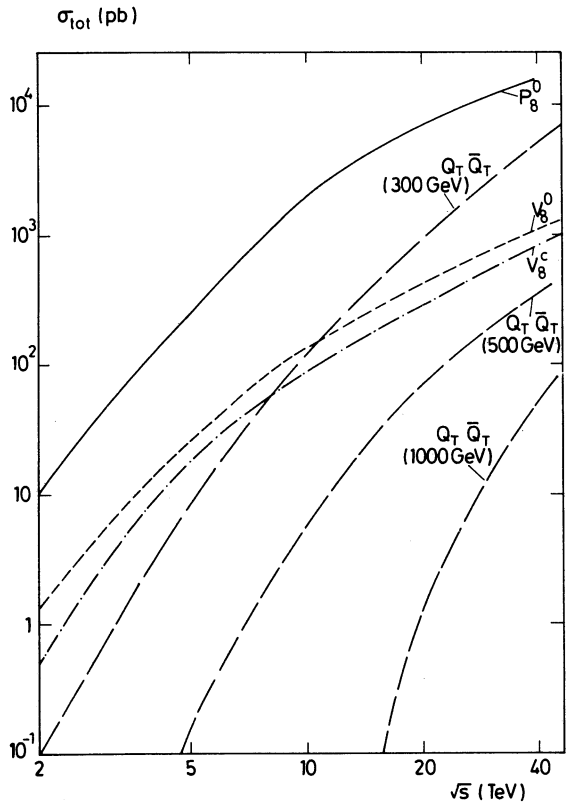

Fig. 42

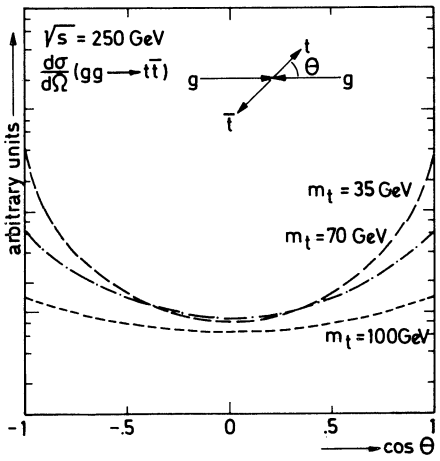

Fig. 43